Cellular/Molecular

Synergy between Electrical Coupling and Membrane Properties Promotes Strong Synchronization of Neurons of the Mesencephalic Trigeminal Nucleus

Sebastian Curti,[1] Gregory Hoge,[2] James I. Nagy,[3] and Alberto E. Pereda[2]

[1]Laboratorio de Neurofisiología Celular, Departamento de Fisiología, Facultad de Medicina, Universidad de la República, Montevideo 11800, Uruguay, [2]Dominick P. Purpura Department of Neuroscience, Albert Einstein College of Medicine, Bronx, New York 10461, and [3]Department of Physiology, University of Manitoba, Winnipeg, Manitoba R3E OJ9, Canada

Electrical synapses are known to form networks of extensively coupled neurons in various regions of the mammalian brain. The mesencephalic trigeminal (MesV) nucleus, formed by the somata of primary afferents originating in jaw-closing muscles, constitutes one of the first examples supporting the presence of electrical synapses in the mammalian CNS; however, the properties, functional organization, and developmental emergence of electrical coupling within this structure remain unknown. By combining electrophysiological, tracer coupling, and immunochemical analysis in brain slices of rat and mouse, we found that coupling is mostly restricted to pairs or small clusters of MesV neurons. Electrical transmission is supported by connexin36 (Cx36)-containing gap junctions at somato-somatic contacts where only a small proportion of channels appear to be open (~0.1%). In marked contrast with most brain structures, coupling among MesV neurons increases with age, such that it is absent during early development and appears at postnatal day 8. Interestingly, the development of coupling parallels the development of intrinsic membrane properties responsible for repetitive firing in these neurons. We found that, acting together, sodium and potassium conductances enhance the transfer of signals with high-frequency content via electrical synapses, leading to strong spiking synchronization of the coupled neurons. Together, our data indicate that coupling in the MesV nucleus is restricted to mostly pairs of somata between which electrical transmission is supported by a surprisingly small fraction of the channels estimated to be present, and that coupling synergically interacts with specific membrane conductances to promote synchronization of these neurons.

Introduction

Electrical synapses constitute a modality of synaptic transmission mediated by clusters of intercellular channels formed by gap junctions at close appositions between neurons (Bennett, 1997). While initially perceived as less prevalent in mammals, electrical synapses are now known to be present in virtually every structure of the brain, where they usually form extensive networks of coupled neurons (Bennett and Zukin, 2004; Connors and Long, 2004; Hormuzdi et al., 2004). Among the first reports on the existence of electrical synapses between mammalian neurons, appearing nearly four decades ago in what are now considered classic experiments, were those focused on the mesencephalic trigeminal (MesV) nucleus of the rat (Baker and Llinás, 1971; Llinás, 1975). The large size of the cell bodies of these primary afferent neurons provided the opportunity to obtain stable intracellular recordings *in vivo*, and to correlate electrophysiological with ultrastructural analysis showing close gap junction-like appositions between these cells (Hinrichsen and Larramendi, 1970; Liem et al., 1991). However, the demonstration of coupling relied on indirect electrophysiological evidence obtained by stimulating the peripheral projections of these afferents at a strength that was subthreshold for the recorded neuron, but was suprathreshold to others, thus allowing the detection of a depolarizing "coupling potential," which represented the electrotonic spread of action potentials from electrically coupled cells (Hinrichsen, 1970; Baker and Llinás, 1971). As a consequence of the experimental design, this indirect approach precluded a detailed analysis of the properties of these electrical contacts. Furthermore, although some somato-somatic membrane specializations ultrastructurally resembled gap junctions (Hinrichsen and Larramendi, 1970; Liem et al., 1991), there is not conclusive evidence that these specializations indeed represent sites for electrical coupling between MesV neurons.

MesV neurons represent an uncommon class of primary afferents because, unlike their counterparts in sensory ganglia, their cell bodies are located within the CNS. Their large, unipolar

Received Dec. 13, 2011; revised Jan. 31, 2012; accepted Feb. 2, 2012.

Author contributions: S.C., G.H., J.I.N., and A.E.P. designed research; S.C., G.H., and J.I.N. performed research; S.C., G.H., J.I.N., and A.E.P. analyzed data; S.C., G.H., J.I.N., and A.E.P. wrote the paper.

This work was supported by Agencia Nacional de Investigación e Innovación (ANII) and Comisión Sectorial de Investigación Científica (CSIC) (S.C.), NIH Grants DC03186 and NS0552827 (A.E.P.), and NIH Grant NS44395 and Canadian Institutes of Health Research (CIHR) (J.I.N.). This work was also supported by the program "Vinculación con Científicos y Tecnólogos Uruguayos Residentes en el Exterior" of ANII, Uruguay. We thank Francisco R. Morales for useful discussions and comments on this manuscript, Dr. B. D. Lynn for genotyping of transgenic mice and help with quantitative analysis of immunofluorescence labeling, B. McLean for excellent technical assistance, and Federico Davoine for generating the MATLAB scripts used for frequency-transfer analysis. We also thank the Morphology Core of the Rose F. Kennedy Center for outstanding support.

Correspondence should be addressed to Sebastian Curti, Department of Physiology, School of Medicine, Universidad de la República, Avenida General Flores 2125, Montevideo 11800, Uruguay. E-mail: scurti@fmed.edu.uy.

DOI:10.1523/JNEUROSCI.6216-11.2012

 0270-6474/12/324341-19$15.00/0

somata are distributed in the brainstem, and their peripheral branches innervate the spindles of jaw closer muscles and mechanoreceptors of periodontal ligaments. The central processes of these cells supply sensory input to neurons of the trigeminal motor nucleus, the rostral parvocellular reticular formation, and the nucleus supratrigeminalis (Dessem and Taylor, 1989; Liem et al., 1991). Also unlike cells in sensory ganglia, the somata of MesV neurons receive synaptic input, which include projections from the hypothalamus and various brainstem structures (Lazarov, 2002; Verdier et al., 2004). Thus, while MesV neurons can be considered functionally and morphologically homologous to neurons of the trigeminal sensory ganglion and dorsal root ganglia, their location within the CNS allows them to participate in complex orofacial physiological processes. That is, subpopulations of these neurons not only mediate the masseteric stretch reflex but may also function as interneurons within more complex neural networks by integrating sensory afferent input with synaptic input from descending systems (Nagy et al., 1986; Kolta et al., 1990; Del Negro and Chandler, 1997). However, the functional contribution of electrical coupling between MesV neurons to this integrative capacity and orofacial motor events remains unknown, partly due to the as yet poorly characterized properties and organization of neuronal coupling in this structure.

By combining tracer-coupling analysis and immunochemistry with current electrophysiological approaches in rodent slices, we examined the properties, organization, and developmental profile of electrical coupling between MesV neurons. We report here that this coupling follows several peculiarities. Rather than extensive, as observed in some structures such as retina (Mills and Massey, 1995; Vaney, 2002) and the inferior olive (Devor and Yarom, 2002), coupling in MesV nucleus was restricted to pairs or small clusters of neurons. In contrast with most examples where coupling decreases or disappears with age (Peinado et al., 1993; Meier and Dermietzel, 2006), coupling in the MesV nucleus is absent during early development and appears at approximately postnatal day 8 (P8) to become an essential feature of the mature cellular phenotype. Furthermore, electrical transmission between MesV neurons is mediated by anatomically distinct somato-somatic contacts, which contain the gap junction protein connexin36 (Cx36). Taking advantage of this uncommon experimental accessibility, we combined imaging-based estimates of numbers of channels present with physiological measurements and found that electrical coupling is supported by a surprisingly small fraction of functional channels. Our data indicate that electrical coupling between MesV neurons can be strong and closely interacts with active membrane properties to promote synchronized activity among pairs of these afferents.

Materials and Methods

Animals were used according to the guidelines of Comisión Honoraria de Experimentación Animal of Universidad de la República (Uruguay), the Institutional Animal Care and Use Committee of Albert Einstein College of Medicine (in accordance with the National Institutes of Health *Guide for the Care and Use of Laboratory Animals*), and the Central Animal Care Committee of University of Manitoba, with minimization of the numbers of animals used.

Slice preparation and electrophysiological recordings. Transverse brainstem slices (250 μm thick) were prepared from Sprague Dawley or Wistar rats (age, P2–P20). Slices obtained using a vibratome (Leica VT 1000s or DTK Microslicer) were placed in cold sucrose solution containing 248 mM sucrose, 2.69 mM KCl, 1.25 mM KH_2PO_4, 26 mM $NaHCO_3$, 10 mM glucose, 2 mM $CaCl_2$, and 2 mM $MgSO_4$. The slices were then transferred to an incubation chamber filled with sucrose solution at room temperature and incubated for 60 min. The sucrose solution was slowly replaced by physiological solution containing 124 mM NaCl, 2.69 mM KCl, 1.25 mM KH_2PO_4, 26 mM $NaHCO_3$, 10 mM glucose, 2 mM $CaCl_2$, and 2 mM $MgSO_4$. Sections were kept at room temperature in the physiological solution until they were transferred into the recording chamber. The recording chamber, mounted on an upright microscope stage (Nikon Eclipse E600), was continuously perfused with physiological solution (1–1.5 ml/min) at room temperature. Whole-cell patch recordings were performed under visual control using infrared differential interference contrast optics (IR-DIC). MesV neurons were identified on the basis of their location, large spherical somata, and characteristic electrophysiological properties in response to both depolarizing and hyperpolarizing current pulses (Liem et al., 1991; Del Negro and Chandler, 1997; Pedroarena et al., 1999). Recording pipettes (6–12 MΩ) were filled with intracellular solution containing 144 mM K-gluconate, 3 mM $MgCl_2$, 0.2 mM EGTA, 4 mM Mg-ATP, 0.3 mM Na-ATP, and 10 mM HEPES, pH 7.2. In some experiments, the Na^+ channel blocker lidocaine *N*-ethyl bromide (QX-314) (1 mM) was added to the intracellular recording solution. The seal resistance between the electrode tip and the cell membrane was >1 GΩ. Simultaneous recordings were made using one Axopatch 200B and one Axoclamp 2A amplifiers or a Multiclamp 700B amplifier (Molecular Devices). Recordings were low-pass filtered at 5 kHz and acquired by means of an analog-to-digital converter connected to a computer, sampled at 20 or 10 kHz depending on the experiment. Data were analyzed using pClamp 9 (Molecular Devices) and Igor (Wavemetrics) software.

Calculation of coupling coefficient. For coupling coefficient (CC) calculations, hyperpolarizing current pulses of 200–400 ms duration were injected into one cell and resulting voltage deflections were measured in both cells. The coupling coefficient from cell 1 to cell 2 (CC_1) was defined as V_2/V_1 and the coupling coefficient in the opposite direction from cell 2 to cell 1 (CC_2) was defined as V_1/V_2, where V_1 is the voltage deflection in one cell and V_2 is the corresponding voltage deflection in the other cell. A total of 10–100 single responses was averaged to improve the signal-to-noise ratio. For each of the coupled pairs, the mean CC was calculated as the average from the values in both directions.

Junctional resistance estimation. The strength of an electrical synapse is influenced by both the gap junctional conductance and the input resistance of the postsynaptic cell (Bennett, 1966). To evaluate the contribution of gap junctional conductance to the CC, the junctional resistance between pairs of MesV coupled neurons (R_C) was estimated following Devor and Yarom (2002) as follows:

$$R_{c1} = \frac{\frac{V_2}{I_2} \times \frac{V_1}{I_1} \times [CC_1 \times CC_2 \times (1 - CC_1) - (1 - CC_1)]}{CC_1 \times \left(\frac{V_2}{I_2} \times CC_2 - \frac{V_1}{I_1}\right)}$$

$$R_{c2} = \frac{\frac{V_1}{I_1} \times R_{c1} \times (1 - CC_2)}{R_{c1} \times CC_2 - \frac{V_1}{I_1} \times CC_2 \times (1 - CC_1)},$$

where R_{C1} and R_{C2} are the values of the junctional resistance from cell 1 to cell 2 and form cell 2 to cell 1, respectively. As defined, I_1 and I_2 are the magnitude of the injected current pulses in each cell, and V_1 and V_2 the corresponding voltage drop in each cell. These estimates assume a simple two-neuron model with passive membrane properties coupled directly by a single junction and does not account for parallel conductance pathways via adjacent coupled neurons or cellular processes.

Junctional conductance determination. To determine junctional conductance, dual voltage-clamp experiments were performed in the presence of specific blockers of the main voltage-dependent conductances of MesV cells [0.5 μM tetrodotoxin (TTX), 1 mM 4-aminopyridine (4-AP), 1 mM CsCl, 0.2 mM $CdCl_2$]. Voltage commands of increasing amplitude in steps of 5 or 10 mV and of both polarities were applied into one of the cells from a holding potential of -50 mV while the other cell was held at -50 mV. The junctional, or synaptic, currents (I_j) were measured in the nonstepped cell (see Fig. 4*D*). Junctional conductance was obtained

from linear regressions (see Fig. 4*E*) according to the following equation: $G_j = (V_1 - V_2) \times I_j$, where G_j is the junctional conductance, V_1 and V_2 are the membrane potentials of cell 1 and cell 2 respectively, and I_j is the synaptic current that flows through the junction.

Frequency-transfer analysis. The transfer properties between pairs of electrically coupled MesV neurons was determined by injecting frequency modulated (2–600 Hz) sine waves of current (50–300 pA) into one of the coupled cells (ZAP protocol), while recording the resulting membrane voltage deflections in both cells (see Fig. 8*A*). ZAP input current was computer-generated according to the following formula: $I(t) = \sin(8.10^{-7} \times t^3)$ (Wu et al., 2001), and peak-to-peak amplitude was adjusted to induce subthreshold voltage deflections. Fast Fourier transform (FFT) was calculated for presynaptic and postsynaptic membrane responses. The frequency-transfer property was determined as the ratio of the postsynaptic FFT over the presynaptic FFT using MATLAB software (MathWorks). Then, transfer was low-pass filtered applying a moving average and decimation algorithms.

Cross-correlation analysis. Cross-correlation functions looking for regularities between two data sets were determined using pClamp 9 software, shifting data sets in both directions, in 0.1 ms increments. For cross-correlation of action potential firing, episodes of 0.5–1 s of steady firing were analyzed, and the *y*-axis of the cross-correlograms, expressed as cross-correlation function index, represents the probability of a spike occurring in a bin given a single spike in the reference trace.

Tracer-coupling. In experiments in which tracer coupling was tested, 0.5% Neurobiotin (Vector Laboratories) was included in the recording pipette and iontophoretically injected using pulses of +500 pA and 250 ms duration every second (1 Hz) over 10 min. After injection, the electrode was removed and slices were incubated at room temperature for 2 h to allow diffusion. Slices were then fixed overnight at 4°C in 4% paraformaldehyde in 0.2 M sodium phosphate buffer. After washing with PBS (Cellgro/Mediatech), slices were washed in PBS containing 5% normal goat serum and 0.3% Triton X-100 (Sigma-Aldrich) and then incubated for 1 h with Alexa Fluor 555-conjugated streptavidin, 2 mg/ml at 1:250 dilution (Invitrogen; S-32355), in PBS containing 3% Triton X-100. Finally, slices were washed in PBS buffer and mounted on microscope slides for confocal analysis. Control experiments were performed by placing a pipette in the extracellular space adjacent to MesV neurons while applying positive pressure to expel Neurobiotin-containing internal solution from the pipette, as would occur during an approach for a whole-cell recording. The slices were then processed for Neurobiotin labeling, as described above. Cells were visualized under confocal microscopy with a Zeiss LSM510 confocal microscope (Zeiss), and the images were processed using Zeiss ZEN software. Optical *z*-section images were collected 1 μm apart to reconstruct the entire somata.

For those cases in which Neurobiotin injections were combined with labeling for Cx36, the fixation time in paraformaldehyde was reduced to 10–40 min. Afterward, slices were washed with PBS, and then, to block nonspecific labeling, were gently shaken for 1 h in PBS containing 0.4% Triton X-100 and 5% normal goat serum (Vector Laboratories; S-1000). At this point, the slices were washed again (PBS with 0.4% Triton X-100) and then incubated overnight at 4°C with a polyclonal anti-Cx36 antibody (Invitrogen; 36-4600) diluted 1:250 in PBS containing 3% Triton X-100 and 5% normal goat serum. Following overnight incubation, the slices were washed in PBS containing 0.4% Triton X-100 and then incubated with secondary antibodies. Neurobiotin was labeled with streptavidin-Alexa Fluor 555 (Invitrogen; S-32355; 2 mg/ml; 1:250), and anti-Cx36 antibody was labeled with goat anti-rabbit Alexa Fluor 488 diluted 1:250 (Invitrogen; A-11008). The slices were then washed in PBS and mounted on microscope slides with antifading mounting medium. Following exposure to Alexa Fluor-conjugated streptavidin and anti-Cx36 antibody, cells were visualized by confocal microscopy using 488 and 543 nm excitation lasers.

Electrophysiology and tracer-coupling in mice. To evaluate the involvement of Cx36 in gap junction-mediated coupling, transverse brainstem slices (300 μm) were prepared from wild-type (WT) C57BL/6 mice and Cx36 knock-out (Cx36 KO) mice (age, P15–P34) developed from C57BL6–129SvEv mixed background (Deans et al., 2001). Slice preparations, recording solutions, microelectrodes, and internal solutions were identical with those used in the rat experiments. Procedures for paired whole-cell recordings and those for intracellular tracer injections with Neurobiotin (Vector Laboratories) were also similar to those described for the rat. For the assessment of tracer-coupling incidence, age-matched groups of wild-type and Cx36 KO mice were tested. Some slices used for analysis of coupling in Cx36 KO mice were examined by immunofluorescence labeling to confirm the absence of Cx36.

Light-microscopic immunofluorescence. For immunohistochemistry, this study used a total of 3 wild-type and 2 Cx36 KO C57BL/6 male mice at postnatal day 9, 6 adult male C57BL/6 wild-type and 3 adult Cx36 KO mice, 4 male rats at postnatal day 15, and 12 Sprague Dawley adult male rats. In our search for connexins expressed by MesV neurons, immunolabeling for each of the known connexins was examined in two wild-type and two Cx36 KO mice at postnatal day 9, two wild-type and two Cx36 KO adult mice, and two rats at postnatal day 15. For this search, a set of >35 antibodies against all connexins was obtained from Life Technologies. This set in some cases included the use of two different antibodies generated against different sequences within individual connexins, as well as the use of both rabbit polyclonal and mouse monoclonal antibodies generated against the same sequence in some of the connexins. Many of these antibodies have been previously characterized for specificity by comparison of immunofluorescence and/or immunoblotting results in wild-type mice versus mice with knock-out of the various connexins. Such characterization has included antibodies against Cx26 (Nagy et al., 2011); Cx30 (Lynn et al., 2011); Cx30.3, Cx31, Cx31.1 (Zheng-Fischhöfer et al., 2006, 2007a,b); Cx32 (Nagy et al., 2003); Cx36 (Li et al., 2004); Cx47 (Li et al., 2008b); and Cx57 (Ciolofan et al., 2007). Similar comparisons between wild-type and connexin KO mice have confirmed the specificity of antibodies against Cx29, Cx37, and Cx40 (J. I. Nagy, unpublished observations). The specificity of antibodies against Cx43 and Cx45 has been established ultrastructurally by showing their detection of these connexins in gap junction plaques (Rash et al., 2001; Li et al., 2008a). Among the remaining connexins, the specification sheets of the manufacturer (Life Technologies) and our own data (J. I. Nagy, unpublished observations) indicate detection of gap junctions in tissues where each connexin is reported to be highly expressed (Cx30.2, intercalated discs in the conduction system of heart; Cx39, gap junctions in embryonic skeletal muscle; Cx46 and Cx50, gap junctions in lens).

Preparation of animals for immunohistochemical studies was performed according to two different protocols involving either transcardiac perfusion or immersion fixation, and sections were processed for immunofluorescence labeling as previously described (Li et al., 2004, 2008a). For perfusion, animals were deeply anesthetized with equithesin (3 ml/kg) and transcardially perfused with ice-cold 50 mM sodium phosphate buffer (PB), pH 7.4, containing 0.9% NaCl, 0.1 sodium nitrite, and 1 U/ml heparin, and then perfused with cold 0.16 M sodium phosphate buffer, pH 7.6, containing 1% freshly depolymerized paraformaldehyde and 0.2% picric acid. Animals were then perfused with ice-cold 25 mM sodium phosphate buffer, pH 7.4, containing 10% sucrose. Volumes of perfusion solutions were delivered at 1 ml/g of body weight. Brains were removed and stored for a minimum of 24–48 h in a cryoprotectant solution consisting of 10% sucrose in PB. Alternatively, for immersion fixation, animals were deeply anesthetized as above, decapitated, and the brains were removed and placed for 20 min into fixative containing 0.16 M sodium phosphate buffer, pH 7.6, 2% freshly depolymerized paraformaldehyde, and 0.2% picric acid. They were then transferred to cryoprotectant as above. Although immersion fixation is often less preferable than cardiac perfusion for most immunohistochemical applications, we have found that it yields superior results for Cx36 detection in some brain regions. Typically, tissues from late postnatal and adult animals were taken after fixation by perfusion, while brains from animals up to postnatal day 10 were immersion fixed.

Tissue sections were cut at a thickness of 15 μm using a cryostat, collected on glass slides, and then washed for 20 min in 50 mM Tris-HCl, pH 7.4, containing 1.5% sodium chloride (TBS) and 0.3% Triton X-100 (TBSTr). Sections were incubated with mouse monoclonal anti-Cx36 for 24 h at 4°C, and then washed for 1 h in TBSTr, and incubated for 1.5 h at room temperature with Cy3-conjugated goat anti-mouse IgG diluted 1:200 (Jackson ImmunoResearch Laboratories). For double immunoflu-

orescence labeling, sections were incubated simultaneously with mouse monoclonal anti-Cx36 in combination with a rabbit antibody against each of the other connexins examined for labeling in MesV nucleus. Sections were incubated with primary antibody for 24 h at 4°C, washed for 1 h in TBSTr, and then incubated for 1.5 h at room temperature simultaneously with Cy3-conjugated goat anti-mouse IgG diluted 1:200 and Alexa Flour 488-conjugated goat anti-rabbit IgG diluted 1:1000 (Invitrogen). All antibodies were diluted in TBSTr containing 5% normal goat or normal donkey serum. After secondary antibody incubations, sections were washed in TBSTr for 20 min, and then washed in 50 mM Tris-HCl buffer, pH 7.4, for 30 min, and covered with antifade medium and coverslipped. Before coverslipping, some sections processed for labeling of Cx36 were counterstained with green Nissl fluorescent NeuroTrace (stain N21480) (Invitrogen). Control procedures included omission of one of the primary antibodies with inclusion of each of the secondary antibodies to establish absence of inappropriate cross-reactions between primary and secondary antibodies or between different combinations of secondary antibodies. Immunofluorescence images were acquired on a Zeiss Axioskop2 fluorescence microscope using Axiovision 3.0 software (Carl Zeiss) and on an Olympus Fluoview IX70 confocal microscope using Olympus Fluoview software (Olympus), and assembled using Adobe Photoshop CS (Adobe Systems), CorelDRAW Graphics Suite 12 (Corel Corporation), and Northern Eclipse software (Empix Imaging).

As an indication of probable coupling between MesV neurons, quantitative analysis of immunofluorescence localization of Cx36 at points of apposition between ensembles of MesV neurons was undertaken using three postnatal day 15 rats and three adult rats. At each age, serial sections were collected from the rostral to the caudal pole of MesV nucleus, and taken for immunolabeling of Cx36 and counterstaining with green fluorescence Nissl stain. The total number of Nissl-stained MesV somata on both the left and right MesV nucleus in each section of each animal was counted. At the same time, counts of the number of pairs, triplets, quadruplets, etc., of consecutively apposed MesV neuronal somata displaying immunolabeling for Cx36 at each of their points of consecutive contacts (as illustrated in Fig. 2*K*,*L*) were conducted using a 40× objective lens. Importantly, the presence of Cx36 at points of MesV neuronal contacts was taken for counts and as a measure of probable coupling, rather than other features of immunolabeling such as intracellular immunoreactivity, which was totally absent in MesV neurons of adult animals. In each animal, the frequency of neurons linked consecutively in series of 2, 3, or greater number of cells was determined and expressed as an average percentage from three animals.

To estimate the average area labeled by anti-Cx36 between pairs of MesV neurons, sections through MesV nucleus from rats at postnatal day 15 were searched for somata that displayed labeling for Cx36 near the center of cell surfaces, which represent en face views of Cx36 immunofluorescence at points of MesV somata contacts in the *z*-axis (as illustrated in Fig. 2*G--J*). Care was taken to insure that labeling occurred at the centers of cell surfaces to ensure capture of the entirety of Cx36 at the apposition. High-magnification confocal images of 10 such appositions were obtained (as illustrated in Fig. 4*A*). The area of each of the individual Cx36-puncta at each apposition was measured using ImageJ (W. S. Rasband, ImageJ, National Institutes of Health, Bethesda, MD; http://imagej.nih.gov/ij/; 1997–2011), and the area of all the puncta at the apposition was summed to give a total puncta area per apposition. The area of a total of 701 puncta was obtained from the 10 images, and the total area of puncta in each image was then averaged over the 10 images to give mean square micrometers ± SEM, with $n = 10$. To minimize halation, during preliminary analyses the gain on the confocal microscope was set from a low level allowing borderline visualization of the smallest, faintest Cx36-positive puncta to an upper but still subsaturating level providing clear visualization of all Cx36-puncta. With increasing levels of gain, the phenomena of halation produced larger diameter puncta, where the average increase in puncta diameter at the highest gain setting used was approximately twofold. To minimize this phenomenon, we chose to capture images at the lower gain setting. This lower setting likely resulted in some degree of halation, causing an overestimate of the brightest of Cx36-puncta diameter, as further reduction of the gain that resulted in loss of the faintest puncta caused a size reduction in the brightest puncta by a factor of 2.

Statistical analysis. Results were expressed as average value ± SD or SEM. Significance of quantitative data was determined by using χ^2 test, and Student's *t* test.

Results

Electrical coupling between pairs of adjacent MesV neurons

We investigated the presence and properties of electrical coupling between adjacent pairs of MesV neurons using paired recordings in slices of rat brainstem visualized by IR-DIC (Fig. 1*A*). These neurons were identified by their large spherical somata and characteristic electrophysiological properties in response to current steps of both polarities (Fig. 1*B*). Suprathreshold responses were characterized by the presence of spikes at the beginning of the current steps that were followed by repetitive discharges of variable duration, while hyperpolarizing responses characteristically evoked prominent sag due to the activation of the I_H current (Khakh and Henderson, 1998). The presence of spontaneous oscillations of the membrane potential that can lead to spike bursting (Fig. 1*B*, bottom panel) provided an additional criterion for the identification of these neurons (Pedroarena et al., 1999; Wu et al., 2001). The input resistance (R_{in}) averaged 109.6 ± 46.6 MΩ (SD) ($n = 132$). The presence of electrical coupling was tested by recording membrane responses in two adjacent MesV neurons following the injection of hyperpolarizing current pulses in one of the cells (the magnitude of the current step was adjusted to produce a voltage drop in the injected cell of ~40 mV or larger). An example of a coupled pair is illustrated in Figure 1*C*, in which a current pulse in the presynaptic cell evokes a membrane response of the same sign in the postsynaptic cell, although of lower amplitude and slower temporal course. Most of the tested pairs (see below) did not show evidence of electrical coupling in either direction (Fig. 1*D*).

The steady-state CC, defined as the voltage drop at the postsynaptic cell divided by the voltage drop at the presynaptic cell measured at the end of the current step (see Materials and Methods), was calculated for each recorded pair. A pair of MesV neurons was considered to be electrically coupled when the steady-state CC was ≥0.005, a criterion determined by the noise of the recording conditions. According to this criterion, only 56 of the 243 tested pairs were electrically coupled (23%; Fig. 1*E*). For each coupled pair, the CC and junctional resistance were estimated (see Materials and Methods) and expressed as the average of the values in both directions. The steady-state CC averaged 0.19 ± 0.14 (SD) (range, 0.0055–0.49; $n = 47$) (Fig. 1*F*, left panel, filled circle and error bars), whereas the junctional conductance averaged 6.2 ± 6.33 nS (SD) (range, 0.009–25.6 nS; $n = 47$) (Fig. 1*F*, right panel, filled circle and error bars). Measurements of coupling coefficient obtained at the initial peak of the voltage responses were slightly bigger than those obtained near the end of the pulse or steady state [0.28 ± 0.21 (SD) vs 0.19 ± 0.14 (SD); $n = 47$; $p < 0.05$]. Because estimates of junctional conductance (see Materials and Methods) from measurements of CC and R_{in} obtained at the initial peak and near end of the pulse of the voltage responses were not significantly different [5.18 ± 5.68 nS (SD) vs 6.2 ± 6.33 nS (SD); $n = 47$; $p = 0.4$], the observed differences in CC are likely ascribable to the impact of the activation of some I_H channels on the R_{in} of the postsynaptic cell by the coupling potential. Consistent with this interpretation, the disparity between these two measurements was more prominent in highly coupled pairs (which evoke larger coupling potentials) than in weakly coupled pairs (data not shown). The strength of

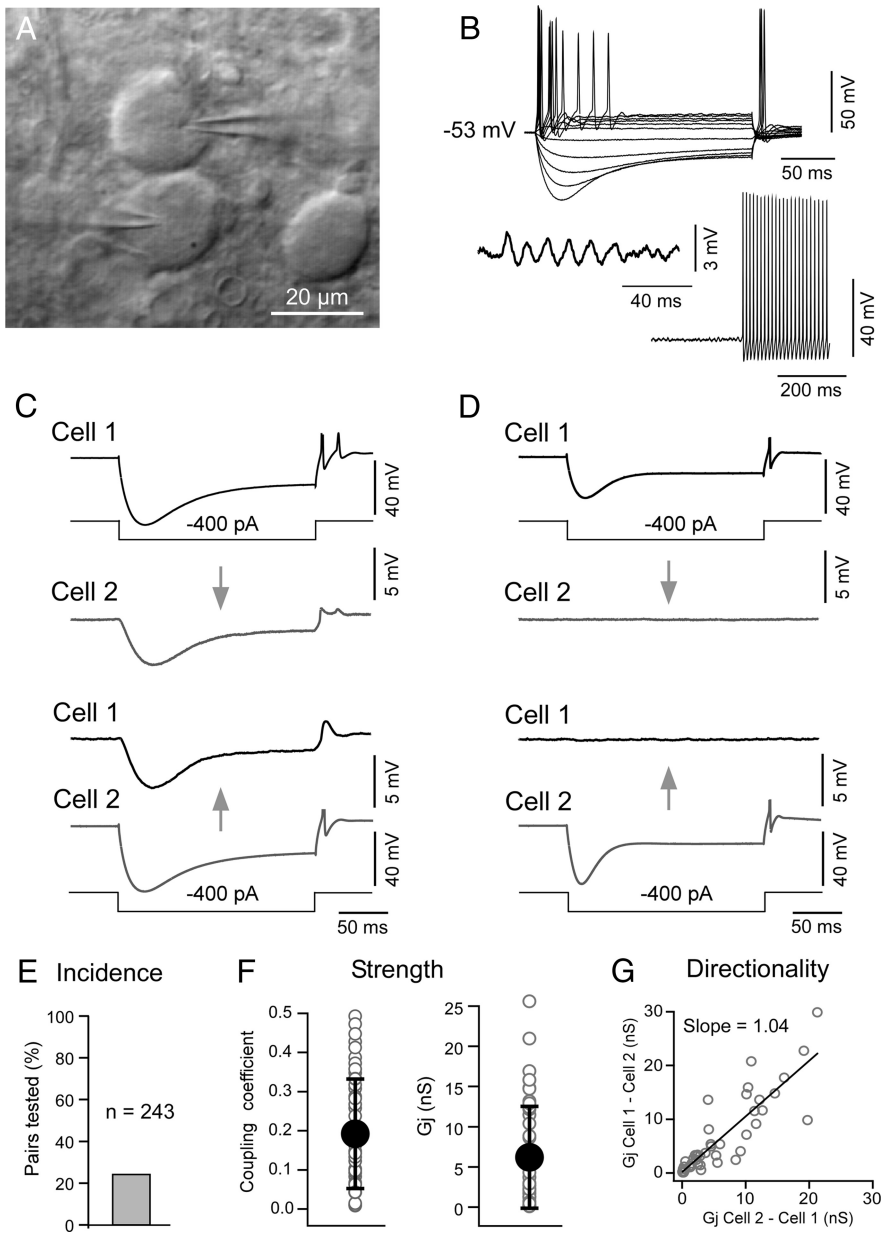

Figure 1. Electrical coupling between pairs of MesV neurons. ***A***, IR-DIC image of a pair of contiguous MesV neurons during a simultaneous whole-cell recording. ***B***, Membrane responses to a family of depolarizing and hyperpolarizing current pulses (above), and examples of spontaneous membrane oscillations and spontaneous repetitive discharges (below), characteristic of MesV neurons. ***C***, Simultaneous recording from a pair of electrically coupled MesV neurons. Voltage responses to 200 ms hyperpolarizing (400 pA) current pulses injected either in cell 1 (top panel) or cell 2 (bottom panel). The CCs measured at steady state (just before the end of the current steps) are 0.057 from cell 1 to cell 2 and 0.055 in the opposite direction. ***D***, Simultaneous recordings from a pair of uncoupled MesV neurons. Note that, in both ***C*** and ***D***, postsynaptic voltage membrane responses are depicted at larger scale than the corresponding presynaptic responses. Presynaptic spikes are illustrated truncated. The traces represent the average of 20 single responses. ***E***, Incidence of electrical coupling ($n = 243$ pairs). ***F***, Strength of electrical coupling between MesV cells. The plots show values of CC (left) and estimates of junctional conductance (right) for the population of coupled cells. Individual (open circles) and average (filled circles) values are illustrated superimposed ($n = 47$; error bars indicate SD). ***G***, Estimates of junctional resistance in both directions (cell 1 to cell 2, and cell 2 to cell 1) are plotted against each other, indicating that most contacts lack significant rectification. The data were fitted with a straight-line function.

electrical transmission in the vast majority of the recorded pairs was bidirectional and symmetric. Figure 1*C* illustrates one of these examples in which the CC was estimated to be 0.057 in one direction (from cell 1 to cell 2; Fig. 1*C*, top panel) and 0.055 in the opposite direction (from cell 2 to cell 1; Fig. 1*C*, bottom panel). Estimates of junctional conductance in both directions for each pair showed a positive correlation with a slope of 1.04 ($R^2 = 0.75$), not significantly different from 1 ($p = 0.7$; Fig. 1*G*), indicating that gap-junctional conductance between MesV neurons is largely nonrectifying (strong asymmetry was find in only 1 of 47 experiments; this experiment lies >3 SDs from the mean and therefore was not included in this analysis). Supporting this conclusion, the difference in the value of junctional conductance in each direction (from cell 1 to cell 2 and vice versa) in these experiments was not significantly different from 0 ($p = 0.9$).

Cx36-containing junctions interconnect MesV neurons

Immunofluorescence labeling for Cx36 is widely distributed at interneuronal gap junctions in adult rodent brain (Nagy et al., 2004; Meier and Dermietzel, 2006), and Cx36 expression is even more widespread in developing brain (Condorelli et al., 1998; Söhl et al., 1998). We investigated by immunohistochemical approaches whether Cx36 is also expressed by MesV neurons and whether it shows a subcellular localization where it could support gap junction-mediated electrical coupling between these neurons.

These studies were undertaken in the MesV nucleus of rats at P15, corresponding roughly to the age at which electrophysiological studies of coupling between MesV neurons were conducted, as well as in the MesV nucleus of adult rats. Images in Figure 2 show immunolabeling for Cx36 with red fluorochrome in sections counterstained with green Nissl fluorescence. At anterior levels through MesV nucleus, neuronal somata are somewhat dispersed along the dorsoventral axis, thus reducing the frequency of contacts between them. Nevertheless, most of these neurons were moderately laden with fine Cx36-positive puncta around their periphery (Fig. 2*A*). At more posterior levels (Fig. 2*B*), the MesV nucleus is much more compact, with constituent somata often appearing in clusters and in close apposition to each other. Immunolabeling for Cx36 was more concentrated within the MesV nucleus than in surrounding regions (Fig. 2*B*). Labeling associated with MesV somata consisted of both fine Cx36-positive puncta around the somata surfaces and large aggregates of puncta at points of contact (Fig. 2*C*). Through focus of entire cells by confocal microscopy revealed that virtually all of the fine dispersed puncta were localized to the cell surface rather than intracellularly (Fig. 2*D*). These puncta varied considerably in size, with diameters ranging from ~0.3 to 1 μm. As shown by confocal analysis (Fig. 2*E*,*F*), immunolabeling at somatic appositions did not consist of a single large immunopositive plaque,

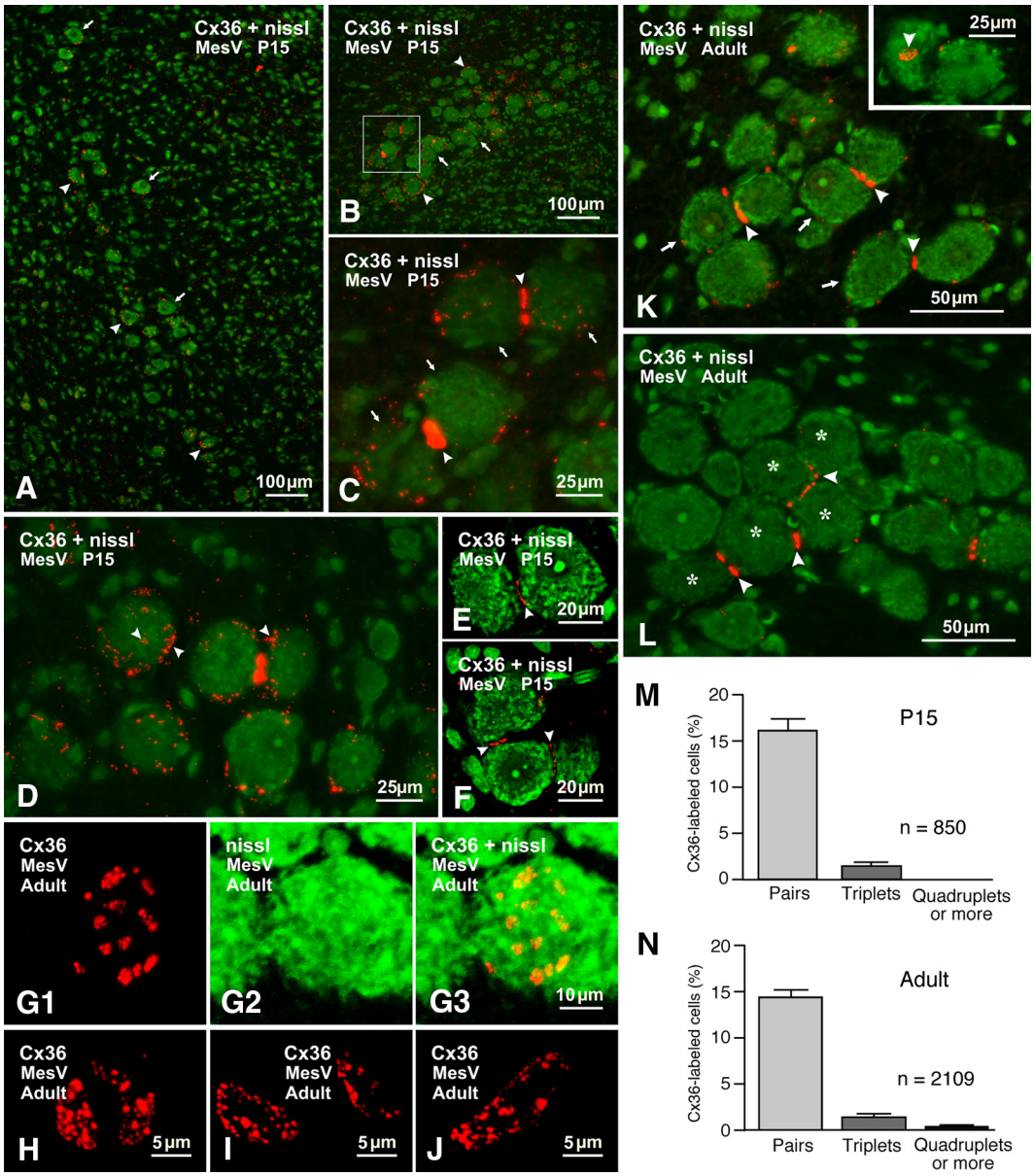

Figure 2. Immunofluorescence labeling of Cx36 associated with MesV neurons at postnatal day 15 and in adult rat brain. In double-labeled panels, labeling for Cx36 is shown with red fluorochrome in sections counterstained for Nissl with green fluorochrome. ***A***, Low magnification at an anterior level of MesV, showing dispersed MesV somata (arrows) decorated on their surface with Cx36-positive puncta (arrowheads). ***B***, MesV at a more posterior level (*z*-stack, 7 μm), showing dense labeling for Cx36 (arrowheads) among clusters of MesV neurons (arrows). ***C***, Higher magnification of the boxed area in ***B*** (*z*-stack, 4 μm), showing labeling for Cx36 (arrowheads) at appositions between pairs of MesV neurons (arrows). ***D***, Single-scan image showing fine dispersed labeling for Cx36 (arrowheads) around the periphery and surface of MesV neurons. ***E***, ***F***, Confocal scan of a pair (***E***) and a triplet (***F***) of MesV neurons in apposition, showing Cx36-puncta along the length of their contacts (arrowheads). ***G–J***, Confocal images showing en face views of labeling for Cx36 at MesV neuronal appositions. The images in ***G*** (*z*-stack, 3 μm) are the same field showing Cx36-puncta (***G1***) on the surface of a MesV neuron (***G2***; overlay in ***G3***) in apposition with another neuron in the *z*-axis. ***H–J***, En face views (*z*-stack, 4 μm) showing clusters of Cx36-puncta displaying various shapes and sizes. ***K***, ***L***, Adult rat showing each of three pairs of MesV neurons (***K***, arrows) linked by Cx36-positive puncta (***K***, arrowheads). The inset in ***K*** shows another pair with one of the neurons displaying en face clustered puncta (arrowhead). A group of five MesV somata (***L***, asterisks) display Cx36-positive puncta at points of apposition with one or two neighbors (***L***, arrowheads). ***M***, ***N***, Quantification of Cx36 labeling at somatic appositions between MesV neurons. The bars illustrate the frequency of Cx36 labeling found at appositions linking pairs, triplets, and groups of four or more MesV somata in rats at postnatal day 15 (***M***; mean ± SD; $n = 850$) and in adult rats (***N***; mean ± SD; $n = 2109$).

but rather of numerous small puncta, which is less evident by standard immunofluorescence microscopy due to halation (light spread) from individual puncta. Aggregates of puncta at somatic appositions were often visualized on edge as in Figure 2, *C*, *E*, and *F*, but were occasionally captured en face, revealing various features of their organization (Fig. 2*G1*,*G3*,*H--J*). Typically, aggregates of these puncta outlined areas that were circular or more often oval in shape, with long and short axes measuring 9–17 and 4–6 μm, respectively, and one to three such aggregates could be seen at somatic appositions. Puncta were unevenly distributed within these aggregates and had a range of sizes (0.3–1.0 μm). Counts of puncta of all sizes within en face views of these aggregates revealed a range of 25–85 puncta per aggregate (see quantification below). Interestingly, MesV neurons toward the end of the second postnatal week displayed a distribution of Cx36-puncta not only in large aggregates at sites of apposition but also as individual or collections of dispersed puncta around their plasma membranes. Since these dispersed puncta were vastly re-

duced in number in adult animals (see below), they may reflect a highly active stage of gap junction formation, involving trafficking and plasma membrane insertion of Cx36, followed by its lateral movement to nascent sites of gap junction formation. Whether other neurons exhibit similar widely dispersed Cx36-puncta on their surface during gap junction formation, which is more readily observable on MesV somata, or whether MesV neurons are unique in this respect remains to be determined.

In adult rat brain, immunolabeling for Cx36 in areas surrounding MesV nucleus was largely absent. Fine Cx36-positive puncta distributed over the surface of MesV somata were still present, but vastly reduced in density. In contrast, robust labeling for Cx36 was more evident at MesV somatic appositions, which consisted either of single puncta or a string of puncta that spanned the entire 7.5–16 μm length of these appositions (Fig. 2*K*). Most frequent was labeling at appositions linking pairs (Fig. 2*K*) or triplets (data not shown) of somata. In the posterior MesV nucleus, containing more densely packed neurons, greater numbers of somata linked in series (five cells in Fig. 2*L*) or in ensembles with individual cells linked to one, two, or three other cells were also encountered. From counts of 850 somata in MesV nuclei of three rats at postnatal day 15, sparse to dense labeling for Cx36 was found at appositions linking 132 pairs of somata (16%) and 12 triplets of somata (1.4%) (Fig. 2*M*). From similar counts of 2109 somata in MesV nuclei of three adult rats, labeling for Cx36 was found at appositions linking 301 pairs of somata (14.3%), 30 triplets of somata (1.4%), and 8 quadruplets or more (0.38%) (Fig. 2*N*). These results almost certainly represent an underestimate of the occurrence of Cx36 at MesV somatic appositions because our examination of 15-μm-thick sections allowed at best visualization of only one-half of the 25–30 μm diameter of MesV somata. Indeed, analysis of serial sections showed that one of a pair of cells linked by Cx36 in one section could be seen to be linked by Cx36 to a third cell in an adjacent section (data not shown). Thicker sections gave weaker immunofluorescence, precluding comparable quantitative analysis involving *z*-stacks in these sections.

MesV neurons are coupled in pairs or small clusters

To investigate the incidence and extent of gap-junctional coupling between MesV neurons, we performed tracer-coupling analysis. Intracellular injection of Neurobiotin in single MesV neurons (Fig. 3*A*,*B*) revealed the presence of coupling in 21% of the injected cells ($n = 98$). In all but two of those cases and despite careful examination by confocal microscopy, Neurobiotin passed to only one adjacent cell from the injected cell (Fig. 3*A–C*). In these other two cases, three cells were found labeled with Neurobiotin, namely the injected cell (identifiable by the higher content of the tracer) and two coupled cells (Fig. 3*E–G*). Functional evidence for the existence of more than two coupled MesV neurons is illustrated in Figure 3*H*. The incidence and extent of tracer coupling (i.e., the percentage and number of coupled cells in those cases in which coupling was observed) are illustrated in Figure 3*D*. Thus, MesV neurons appear to be coupled in pairs or small clusters. However, despite our best attempt at signal amplification during image processing, it is possible that very low levels of Neurobiotin remain undetected in other neighboring cells. In contrast to the finding with Neurobiotin, dye coupling was not detected after single-cell injections of Lucifer yellow ($n = 12$), which invariably resulted in labeling of only the injected cell (data not shown).

The incidence of tracer coupling seemed unexpectedly low in comparison with the high levels of Cx36 detected between MesV neurons. To investigate the relationship of Cx36 immunolabeling among MesV neurons and the occurrence of coupling between these neurons, we performed experiments in which Neurobiotin injections were combined with immunolabeling for Cx36. As illustrated in Figure 3, *I* and *J*, Cx36 labeling was found in the area of contact between pairs of tracer-coupled cells. However, in several cases, tracer coupling was not detected despite the presence of punctate labeling for Cx36 between adjacent pairs of MesV neurons ($n = 3$) (Fig. 3*K–N*), suggesting that channels formed by Cx36 between these neurons could be closed.

Electrical coupling is supported by a small fraction of open gap junction channels

Cx36 labeling was restricted to areas of somato-somatic contacts, providing support for the notion that these membrane specializations represent sites for electrical coupling between MesV neurons. Taking the advantage of the uncommon possibility of identifying the junctional area between two neurons (most electrical coupling in mammalian neurons generally occurs at remote dendro-dendritic contacts) (Connors and Long, 2004), we estimated the average fraction of open channels responsible for electrical coupling between MesV neurons. For this purpose, we first calculated the average area of labeling for Cx36 at somato-somatic contacts. As determined from en face views of Cx36 immunofluorescence at contact sites between MesV somata (Fig. 4*A*), the average number of Cx36-puncta per apposition was 70.1 ± 9.9 (SEM), the puncta diameter was 0.34 ± 0.09 μm (SEM), and the average puncta area was 0.36 ± 0.028 μm^2 (SEM) ($n = 10$). From these measurements, we calculated the total Cx36-labeled area (area of all puncta) per apposition, which averaged 25.5 ± 3.9 μm^2 (SEM) (Fig. 4*B*). Assuming that connexons in gap junction plaques between MesV neurons are organized in a crystalline fashion, where the density is reported to be 12,000 connexons/μm^2 (Kamasawa et al., 2006), the labeled area corresponds to ~306,000 channels. We next obtained direct measurements of junctional conductance from pairs of coupled cells by using the dual whole-cell patch-clamp technique. In contrast with other neuronal types, the somatic location of gap junctions and spherical geometry of MesV neurons contribute to alleviate space clamp limitations. Current responses to voltage steps in a presynaptic neuron were recorded in a coupled MesV neuron (Fig. 4*D*), and the junctional conductance was obtained from the slope of *V*–I relationships (Fig. 4*E*) (see methods). Junctional conductance averaged 2.8 ± 2.0 nS (SD), $n = 8$ (Fig. 4*C*). In four pairs, in which conductance was estimated in both directions, the values were largely symmetrical (Fig. 4*F*), indicating the lack of significant rectification at these contacts, as also found from analysis in current-clamp mode (Fig. 1*G*). Because the single-channel conductance of gap junction channels formed by Cx36 was reported to be 10–15 pS (Srinivas et al., 1999b; Teubner et al., 2000), the average number of open gap junction channels was of 190–280. Given that the opening probability of functional gap junction intercellular channels was reported to be close to 1 (Srinivas et al., 1999a), the estimate indicates that, on average, only 0.06–0.09% of gap junction channels between MesV neurons are functional. Independent estimates of junctional conductance between the same pairs of MesV neurons using indirect approaches that involve measurements of CC and R_{in} (see Materials and Methods) averaged 7.3 ± 5.0 nS (SD) ($n = 9$), representing 0.16–0.24% of the total population of channels, provided independent support for the notion of a very low fraction of open channels contribute to electrical coupling. This value is also con-

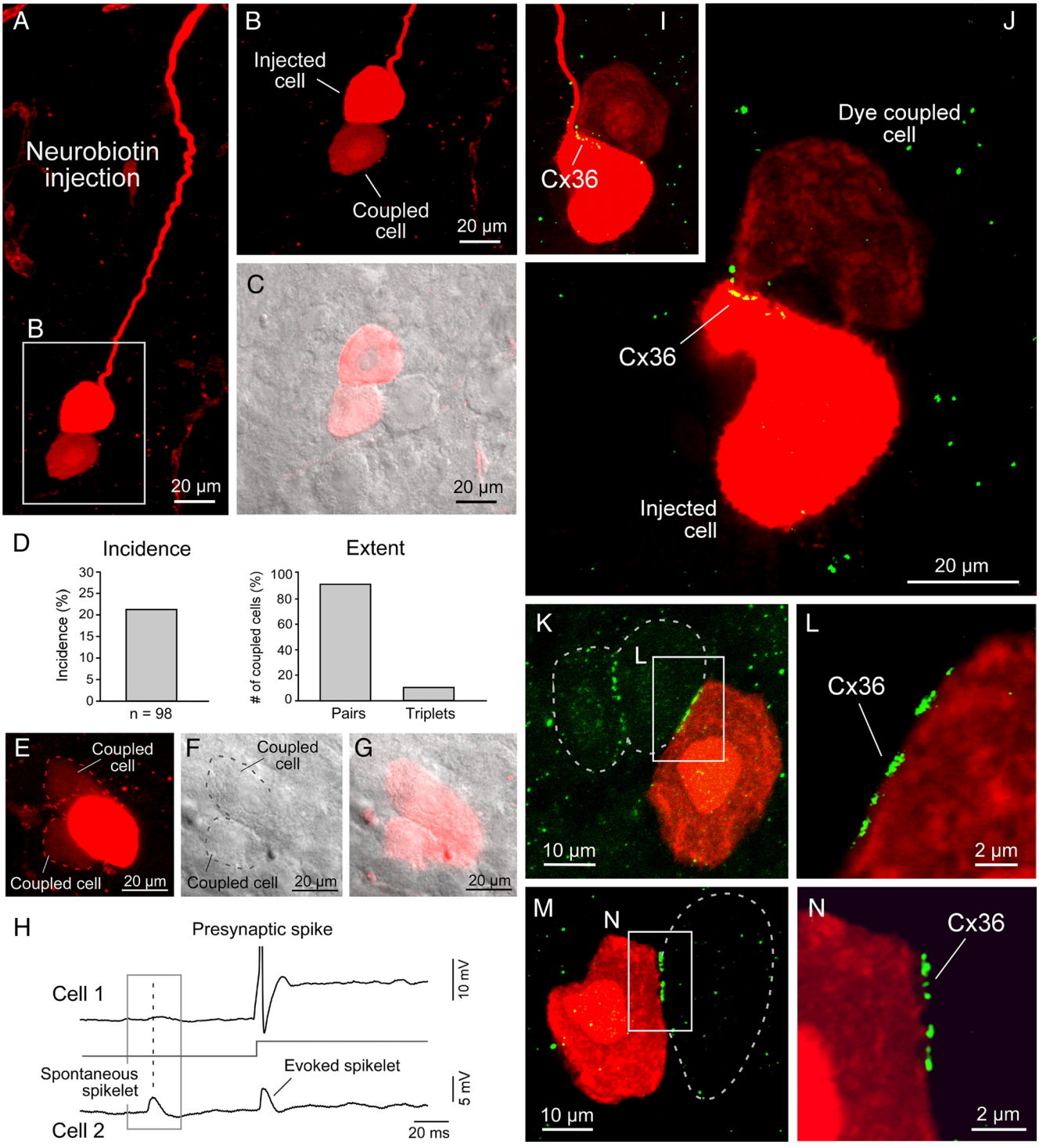

Figure 3. MesV neurons are coupled in small clusters of cells linked by Cx36 at cell– cell appositions. ***A***, Injection of Neurobiotin in a MesV neuron (note the size, morphology, and long processes characteristic of these cells) reveals coupling with immediately adjacent neurons (*z*-stack, 20 μm). ***B***, Magnification of the boxed area in ***A***. ***C***, Confocal image in ***B*** was superimposed with DIC image of the same area. An immediately adjacent cell does not exhibit labeling for Neurobiotin. ***D***, Summary plots of the incidence and extent of tracer coupling, which was detected in ~20% of Neurobiotin-injected neurons (left panel) and in most cases was restricted to one neuron (pairs) (right panel). ***E–G***, Example in which coupling to two other neurons was observed. Confocal image (*z*-stack, 10 μm) of a Neurobiotin-injected MesV neuron (***E***). Shown are DIC of the same area (***F***) and superposition of confocal and DIC images (***G***). The dotted lines denote the perimeter of the coupled cells. ***H***, Simultaneous recording of a pair of electrically coupled MesV neurons. Activation of cell 1 by a suprathreshold depolarizing current pulse evokes a corresponding spikelet in cell 2. The membrane potential of cell 2 also exhibits a spontaneous spikelet that is not correlated with an action potential in cell 1, indicating that cell 2 was coupled with at least one other cell. ***I***, ***J***, Correlation of tracer coupling with Cx36 labeling. The images show the area of contact between two tracer-coupled cells, as revealed by Cx36 labeling (*z*-stacks, 5 μm in ***I*** and 3 μm in ***J***). ***K***, Combination of Neurobiotin injection and Cx36 labeling reveals the lack of tracer-coupling between adjacent neurons displaying Cx36 labeling at appositions (*z*-stack, 5 μm). The dotted lines indicate the perimeter of Neurobiotin-negative MesV neurons. ***L***, Magnification of the boxed area in ***K*** from a single *z*-section. ***M***, ***N***, Another example of lack of tracer coupling between Cx36-containing MesV neurons (single *z*-section).

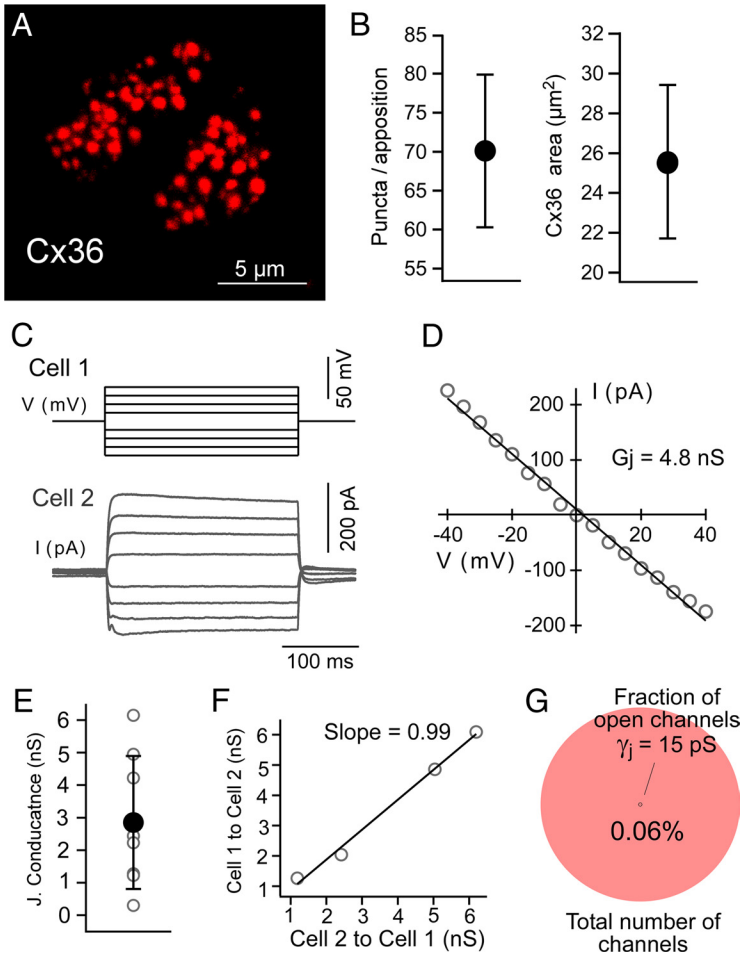

Figure 4. A small proportion of open gap junction channels supports electrical coupling between MesV neurons. ***A***, Confocal immunofluorescence en face views (*z*-stack, 4 μm), showing examples of Cx36-immunopositive clusters used for quantitation of Cx36-puncta area at appositions between MesV neurons. ***B***, Average of Cx36 labeling area per apposition. ***C***, Current traces obtained under dual whole-cell voltage-clamp configuration. Both cells were held at −50 mV, and voltage commands of increasing magnitude in steps of 5 mV of both polarities were applied to one of the cells (cell 1, above), while monitoring junctional current in the second cell (cell 2, below). The transient component observed in response to strong positive voltage commands corresponds to an undetermined voltage-dependent conductance of the presynaptic cell that is not blocked by TTX or K^+ channels blockers. ***D***, Graph of junctional current (ordinates) versus transjunctional voltage (abscissa) for the recordings depicted in ***C***. The data were fitted to a straight-line function, and the junctional conductance (G_j) was determined from the slope of this linear regression (4.8 nS in this pair). ***E***, Estimates of junctional conductance obtained under voltage-clamp configuration. Individual (open circles) and average (filled circles) values are illustrated superimposed (error bars indicate SD). ***F***, Estimates of junctional conductance determined in both directions (cell 1 to cell 2 and cell 2 to cell 1) are plotted against each other obtained from four coupled pairs. Data were fitted to a straight-line function with a slope near 1, indicating the absence of significant rectification at these contacts. ***G***, The diagram illustrates the average proportion of open gap junction channels in appositions between MesV neurons. The area under the pink circle represents the total number of Cx36 intercellular channels per apposition (306,000; 100%) estimated from the average Cx36 labeling area depicted in ***B*** and assuming a density of 12,000 connexons/μm^2. The black dot represents the average number of open channels (190–280, representing the 0.09–0.06% of the average population), according to estimates of macroscopic junctional conductance (***D***) and assuming a unitary conductance (γ_j) of 10–15 pS. The estimate also assumes an open probability of ~1 for intercellular gap junction channels.

sistent with estimates obtained with current clamp for all the coupled pairs (Fig. 1*F*).

Coupling is reduced by gap junction blockers and in Cx36 knock-out mice

To confirm that gap junctions mediated electrical coupling, we investigated the effects of blockers of these channels while monitoring the voltage responses in paired recordings of MesV neurons. As illustrated in Figure 5*A*, the CC was dramatically reduced following application of the gap junction blocker meclofenamic acid (200 μM), which was shown to block both electrical and tracer coupling in retina (Pan et al., 2007; Veruki and Hartveit, 2009), averaging 11.3 ± 15.0% (SD) of control ($n = 8$; $p < 0.05$) (Fig. 5*B*).

Our immunochemical evidence supports the notion that gap junctions between MesV neurons contain Cx36. To confirm its involvement, we investigated the presence of electrical coupling in Cx36 KO mice. Labeling of Cx36 in WT mice was similar to that obtained in the MesV nucleus of the rat (Fig. 5*C*), including observations of aggregates of multiple puncta at somatic appositions (data not shown), although the number of MesV somata appeared far fewer in mouse compared with rat. This labeling was absent in the Cx36 KO mice (Fig. 5*D*). We found that the incidence of tracer and electrical coupling in WT mice was higher than that found in rats, averaging 63% in both cases (Fig. 5*E*). Although markedly reduced (~50%), both tracer and electrical coupling were detected in Cx36 KO mice, averaging 36 and 33%, respectively ($p < 0.05$ and $p < 0.01$, respectively, when compared with WT). The strength of electrical coupling was also reduced, averaging 0.10 ± 0.071 (SD) and 0.032 ± 0.029 (SD) in WT and Cx36 KO mice ($p < 0.01$), respectively (Fig. 5*F*). The "overall strength" of coupling, defined as the product of the incidence and the strength of electrical coupling, was reduced by ~80% (Fig. 5*G*), averaging 6.3 and 1.11 for WT and Cx36 KO, respectively. In contrast to incidence and strength, the extent (number of coupled cells) was not affected in the Cx36 KO mice, when tested with tracer coupling. Both WT and Cx36 KO animals were coupled in pairs, triplets, and in much less degree (one case in WT) quadruplets (Fig. 5*H*), and their relative frequency was not different between these two groups of animals ($p = 0.62$) (Fig. 5*I*). Thus, despite the profound overall reduction in coupling in Cx36 KO mice, the frequency of coupled pairs or small clusters was not affected, indicating that this pattern of coupling cannot be explained by factors such as tracer diffusion time and suggesting that it truly represents the functional organization of electrical coupling in the MesV nucleus, which is maintained in the presence of presumably another connexins.

Although markedly reduced, the persistence of coupling in Cx36 KO mice was surprising given confirmation of the total absence of Cx36. It is unclear whether this coupling is "residual" (i.e., it represents the presence of an additional connexin in the WT) or, on the other hand, represents the induction of a connexin in the Cx36 KO mice that is not normally present in the WT. These two possibilities could not be resolved by immunofluorescence labeling because as in wild-type mice and in rat,

appositions between MesV neurons in Cx36 KO mice at postnatal day 9 and in adult did not display any immunolabeling for connexins that so far have been reported to be expressed in neurons of adult brain (i.e., Cx30.2, Cx45, and Cx57), nor did these apposition display labeling for some connexins found in various peripheral cell types (Cx30.3, 31.1, Cx31, Cx37, Cx39, Cx40, Cx46, Cx50) (data not shown). By immunofluorescence, it was somewhat more difficult to exclude connexins expressed in glial cells (Cx26, Cx29, Cx30, Cx32, Cx43, and Cx47) as candidates for the mediation of coupling between MesV neurons in Cx36 KO mice because, as elsewhere in brain, labeling for these connexins was dense and localized to glial elements in and around the MesV nucleus. Although immunofluorescence examination could not exclude the possibility that some fine punctate labeling for these glial connexins was associated with MesV somatic plasma membranes in either WT and/or Cx36 KO mice, none showed a pattern of labeling at MesV somatic appositions displayed by Cx36 (data not shown). Therefore, the presence of coupling in Cx36 KO mice is unlikely to significantly modify our estimates of number of functional channels (see above) because (1) coupling in null mice could represent a compensatory mechanism, and (2) no other connexin appeared to be present in any significant quantities at MesV neuronal appositions.

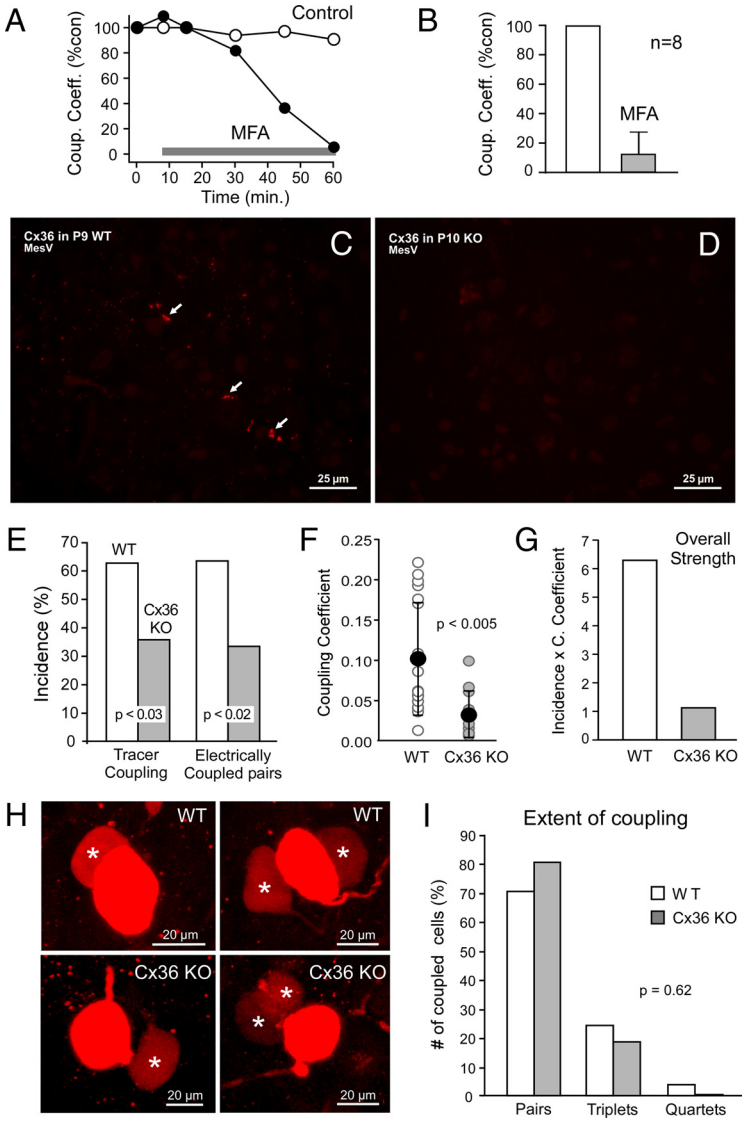

Figure 5. Coupling between MesV neurons was suppressed by gap junction blockers and reduced in Cx36 KO mice. ***A***, Values of CC versus time for two pairs of MesV neurons, in the absence (open circles) and the presence (filled circles) of meclofenamic acid (MFA) (application of MFA is indicated by the gray bar). ***B***, Summary of CCs obtained 40 – 60 min after MFA application, expressed as percentage of control (error bars indicate SD). ***C***, Immunofluorescence labeling of Cx36 at postnatal day 9 in WT mouse, showing Cx36 associated with MesV neurons (arrows), as well as dispersed Cx36-puncta throughout the field. ***D***, A similar field of MesV as in ***C***, but in Cx36 KO mice at postnatal day 10, showing absence of immunolabeling for Cx36. ***E***, Incidence of tracer and electrical coupling in WT and Cx36 KO mice. Tracer coupling (left) averaged 63% in the WT ($n = 38$ injected cells) versus 36% in the Cx36 KO ($n = 44$) ($p < 0.05$). Electrical coupling (right) averaged 63% in the WT ($n = 30$) versus 33% in the Cx36 KO ($n = 40$; $p < 0.01$). ***F***, Values of CC in WT and Cx36 KO mice, showing individual (open circles) and average (black circles) values ($n = 18$ for the WT and $n = 12$ for Cx36 KO; error bars indicate SD; $p < 0.01$). ***G***, Overall strength of electrical coupling for WT and Cx36 KO mice, expressed as coupling incidence multiplied by mean CC. ***H***, Tracer coupling in WT (top panels) and Cx36 KO (bottom panels) mice (*z*-stacks, 5–10 μm). MesV neurons in both WT and Cx36 KO were coupled to one (left) or two (right) neurons (asterisks). ***I***, Extent of coupling in the MesV nucleus of WT and Cx36 KO mice, showing the number of coupled pairs, triplets, and quartets of neurons expressed as percentage of the total number of coupled neurons.

Coupling in the MesV nucleus is developmentally regulated

To investigate the developmental profile of electrical coupling between MesV neurons, we performed tracer-coupling experiments in rats between P2 and P17 (Fig. 6). Surprisingly, and in contrast with most mammalian brain structures (Peinado et al., 1993), coupling was absent during early development (Fig. 6*A*). Coupling appeared at postnatal day 8, almost in a steplike fashion with an incidence of ~22% ($p < 0.05$) between ages P8 and P17 (Fig. 6*A*) (Table 1). The development of coupling paralleled the development of the ability of the explored MesV neurons to undergo repetitive firing (Fig. 6*A*). MesV neurons between P2 and P6 of age were only capable of eliciting a single action potential regardless of the magnitude of depolarizing current (Fig. 6*A*, left inset), whereas they exhibit a robust burst of action potentials after P8 (Fig. 6*A*, right inset) (Wu et al., 2001). The results obtained with tracer coupling were supported by immunofluorescence examination of Cx36 in the MesV nucleus at P5. Fine Cx36-puncta were observed interspersed among MesV neurons, as well as in surrounding areas, including the locus ceruleus located immediately adjacent and medial to MesV nucleus (Fig. 6*B*). Many of the puncta in MesV nucleus did not appear to be associated with large somata, which instead displayed largely intracellular and perinuclear labeling that had a granular appearance, suggesting association with intracellular membraneous structures, perhaps endoplasmic reticulum or Golgi apparatus (Fig. 6*C*). Despite already large areas of contacts between MesV somata at P5, only rarely were small patches of labeling for Cx36 seen at appositions between these somata (Fig. 6*C*, inset). The CC was not systematically explored in this experimental series, preventing us from determining potential developmental changes of the strength of electrical connections (Parker et al., 2009).

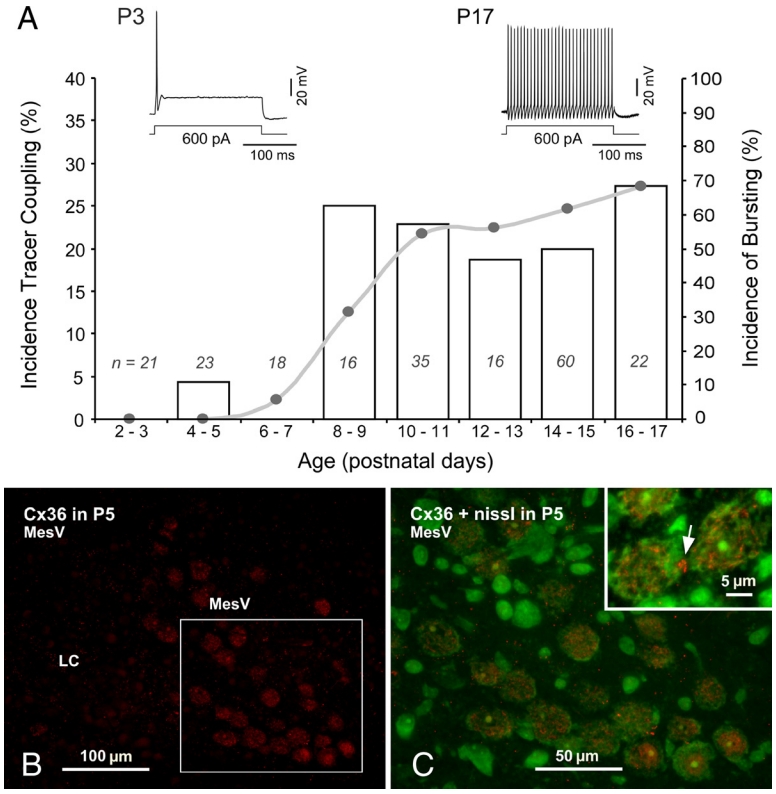

Figure 6. Coupling between MesV neurons increases with age. ***A***, Graph illustrates the incidence of tracer-coupling (bars, left ordinate) as a function of the postnatal age. Coupling was absent during early development, appeared at P8, and remained the same at older ages (~20%; Table 1); n = number of Neurobiotin-injected neurons at each age. Development of coupling parallels development of action potential bursting (connected dots, right ordinate). Bursting was defined as the presence of two or more spikes in response to a current pulse (200 ms in duration) twofold the threshold intensity eliciting a single spike. Insets, Examples of membrane responses to depolarizing current pulses eliciting only a single action potential at P3 (left), and eliciting vigorous repetitive discharges at P17 (right). ***B***, Immunofluorescence labeling for Cx36 in the MesV nucleus at P5 showing fine punctate labeling throughout the field including the locus ceruleus (LC) adjacent to the MesV nucleus. MesV neurons show moderate labeling intracellularly. ***C***, Magnification of the boxed area in ***B***, with Cx36 (red) and fluorescence Nissl counterstaining (green). Labeling for Cx36 is distributed intracellularly, and only very rarely at contacts areas between adjacent somata (inset, arrow).

Active membrane mechanisms enhance electrical coupling

Both electrical coupling and intrinsic membrane properties responsible for repetitive firing develop simultaneously, suggesting they functionally interact. In fact, subthreshold Na^+ currents, such as those responsible for repetitive firing in MesV neurons (Wu et al., 2001), were shown to amplify coupling potentials (known as "spikelets") evoked by presynaptic spikes in a voltage-dependent fashion (Mann-Metzer and Yarom, 1999; Curti and Pereda, 2004; Dugué et al., 2009). We investigated this possible voltage dependency in pairs of electrically coupled MesV neurons. As illustrated in Figure 7*A*, a large depolarizing current pulse in the "presynaptic" cell evoked a strong depolarization that triggered a repetitive discharge, which was simultaneously followed by a depolarizing coupling potential and corresponding spikelets in the postsynaptic cell (bottom panel). As a result of filtering by the membrane properties of the postsynaptic cell (Bennett, 1966; Connors and Long, 2004), spikelets were much smaller in amplitude and typically exhibited a slower temporal course; this property can be appreciated in Figure 7*B*, where the first presynaptic spike and its corresponding postsynaptic coupling potential are illustrated after normalization. [Because of the slow time constant of most mammalian neurons, transmission across electrical synapses of presynaptic signals with high-frequency content, such as the upstroke of an action potential, are greatly attenuated; this attenuation of signals based on their frequency content is usually referred as the "low-pass" filter properties of electrical synapses (Bennett and Zukin, 2004; Connors and Long, 2004).] We found that the amplitude of these spikelets critically depended of the membrane potential of the postsynaptic cell and it was enhanced by depolarizations produced by current injection (Fig. 7*C*), eventually triggering an action potential. The amplitude of the spikelets exhibited a positive correlation with the membrane potential of the postsynaptic cell, indicating a marked voltage-dependent amplification (Fig. 7*C*, right panel). The range of this voltage-dependent amplification is consistent with the activation of a persistent Na^+ current, which is a prominent feature of MesV neurons (Wu et al., 2001). Consistently, this amplification was not observed when QX-314 (1 mM) was added to the postsynaptic recording electrode solution (Fig. 7*D*, left panel). The amplitude of the spikelet at depolarized membrane potentials (approximately −50 mV), expressed as percentage of its amplitude at resting membrane potential, averaged 130.1 ± 14.9% (SD) in control conditions and 95.3 ± 10.4% (SD) in the presence of QX-314 ($p < 0.01$; $n = 5$) (Fig. 7*D*, right panel). Thus, the amplification of depolarizing coupling potentials by a QX-314-sensitive current (likely a persistent Na^+ current) suggests a relevant contribution of active membrane conductances in regulating the efficacy of electrical transmission between MesV neurons.

Frequency-transfer properties of electrical coupling between MesV neurons

To explore the contribution of active membrane conductances in determining the efficacy of electrical coupling, we characterized the transmission of signals as a function of their frequency. For that, frequency-modulated sine wave currents (2–600 Hz; ZAP protocols; see Materials and Methods) were injected into one cell of an electrically coupled pair (Fig. 8*A*, top panel) while monitoring membrane potential variations in both cells (Fig. 8*A*, bottom panel). This protocol evoked membrane responses in the presynaptic (injected) cell that were consistent with previously described resonant properties of MesV neurons (Wu et al., 2001) and that were characterized by an enhancement of voltage responses for frequencies between 20 and 100 Hz (Fig. 8*A*). Membrane responses in the postsynaptic cell were comparable with presynaptic responses, although smaller in amplitude (Fig. 8*A*). Bode plot (magnitude and phase) of frequency-transfer characteristics, defined as the ratio of the postsynaptic FFT over the presynaptic FFT, were constructed for seven coupled pairs (see Materials and Methods) (Fig. 8*B*). The transfer of presynaptic voltage responses was markedly attenuated at high frequencies, with an apparent corner frequency (defined as the intersection of the slope of the attenuation observed at high frequencies and a

Table 1. Incidence of tracer coupling between MesV neurons at different ages

	Age							
	P2–3*	P4–5*	P6–7*	P8–9*†	P10–11*†	P12–13*†	P14–15*†	P16–17*†
Percentage (%)	0%	4%	0%	25%	23%	19%	20%	27%
No. with coupling	0	1	0	4	8	3	12	6
$n =$	21	23	18	16	35	16	60	22
						$p = 0.95$		
				$p < 0.05$				

*$p = 0.9$; †$p < 0.05$.

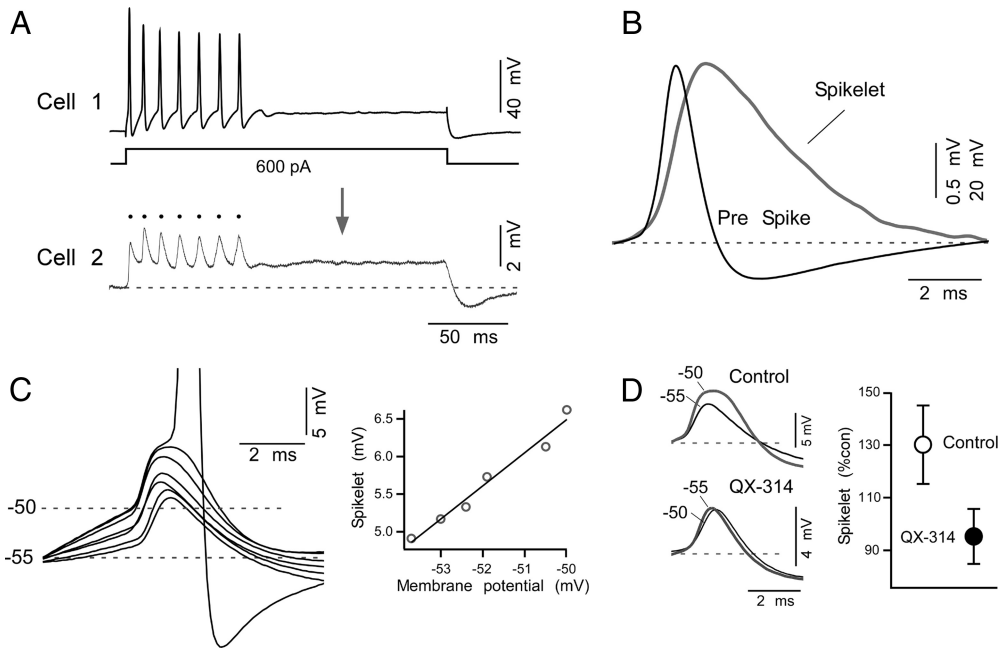

Figure 7. Coupling of action potentials between MesV neurons. ***A***, Injection of a depolarizing current pulse in cell 1 (200 ms in duration, 600 pA in amplitude) evokes a repetitive discharge, and a corresponding coupling potential in cell 2. Note that the longer depolarization produced by the pulse was less attenuated than the shorter lasting presynaptic action potentials (dots). ***B***, The coupling of action potentials ("spikelets") also exhibited a slower time course. Superimposed traces of the first presynaptic action potential (Pre Spike) and the first postsynaptic spikelet (Spikelet) in ***A*** are represented normalized. ***C***, Postsynaptic spikelets show voltage-dependent amplification. Left, Superimposed traces illustrate spikelets obtained at different postsynaptic membrane potentials. Voltage-dependent amplification eventually led to firing of the postsynaptic neuron. Right, Plot of the spikelet amplitude versus membrane potential showing the progressive amplitude increase with depolarization. Data were fitted with a straight-line function. ***D***, Voltage-dependent amplification was prevented by the Na^+ channel blocker QX-314. Left, Superimposed traces correspond to spikelets recorded at resting membrane potential (−55 mV) and at −50 mV, in control conditions (top panel) and when using a QX-314-containing electrode in the postsynaptic cell (bottom panel). Right, Average amplitude of spikelets recorded at depolarized membrane potential during control conditions (open circle) and when the postsynaptic cell was recorded with a QX-314-containing electrode (black circle), expressed as percentage of their respective values at resting potential ($n = 5$; $p < 0.01$).

horizontal line representing the value observed in DC) of 80 Hz and a slope of −24 dB/decade.

Remarkably, the amplitude of the transfer was higher at frequencies near 50 Hz than that obtained with DC signals (Fig. 8*B*, arrowhead), indicating that transmission of electrical signals between MesV neurons exhibits some degree of frequency preference and therefore does not behave as simple "low-pass" filter. Frequency preference in neurons results from the interaction of passive membrane properties with active resonant conductances, typically subthreshold K^+ conductances, and is amplified by persistent Na^+ currents (Hutcheon and Yarom, 2000; Wu et al., 2001; Curti et al., 2008). The addition of TTX (0.5 μM) to the extracellular solution resulted in a reduction of the amplitude of the transfer, particularly for the values around 50 Hz, indicating the participation of Na^+ conductances in improving transmission at those frequencies (Fig. 8*C*). The subsequent addition of 4-AP (1 mM), a blocker of A-type as well as other K^+ conductances, further reduced the amplitude of the transfer of signals with frequencies between 10 and 300 Hz relative to DC, resembling now the properties of a simple "low-pass" filter (Fig. 8*C*). The contribution of the TTX- and 4-AP-sensitive conductances to the transfer of electrical signals is illustrated in Figure 8*E*, in which the subtraction between frequency-transfer responses obtained in control conditions and during the combined application of TTX and 4-AP (colored area) is illustrated superimposed in one of these experiments. TTX- and 4-AP-sensitive conductances also significantly contributed to improve the phase lag between presynaptic and postsynaptic responses. The phase lag at ~50 Hz (peak of transfer amplitude) was found to increase from ~30° in control conditions to 60° in the presence of TTX and 4-AP (Fig. 8*D*). The effect on phase lag was more prominent for signals with frequencies in the 10–100 Hz range (Fig. 8*D*). Consistent with a role of active conductances in the frequency-transfer properties of these electrical synapses, the frequency attenuation properties of MesV neurons were qualitatively different from those reported for neocortical fast-spiking (FS) and low

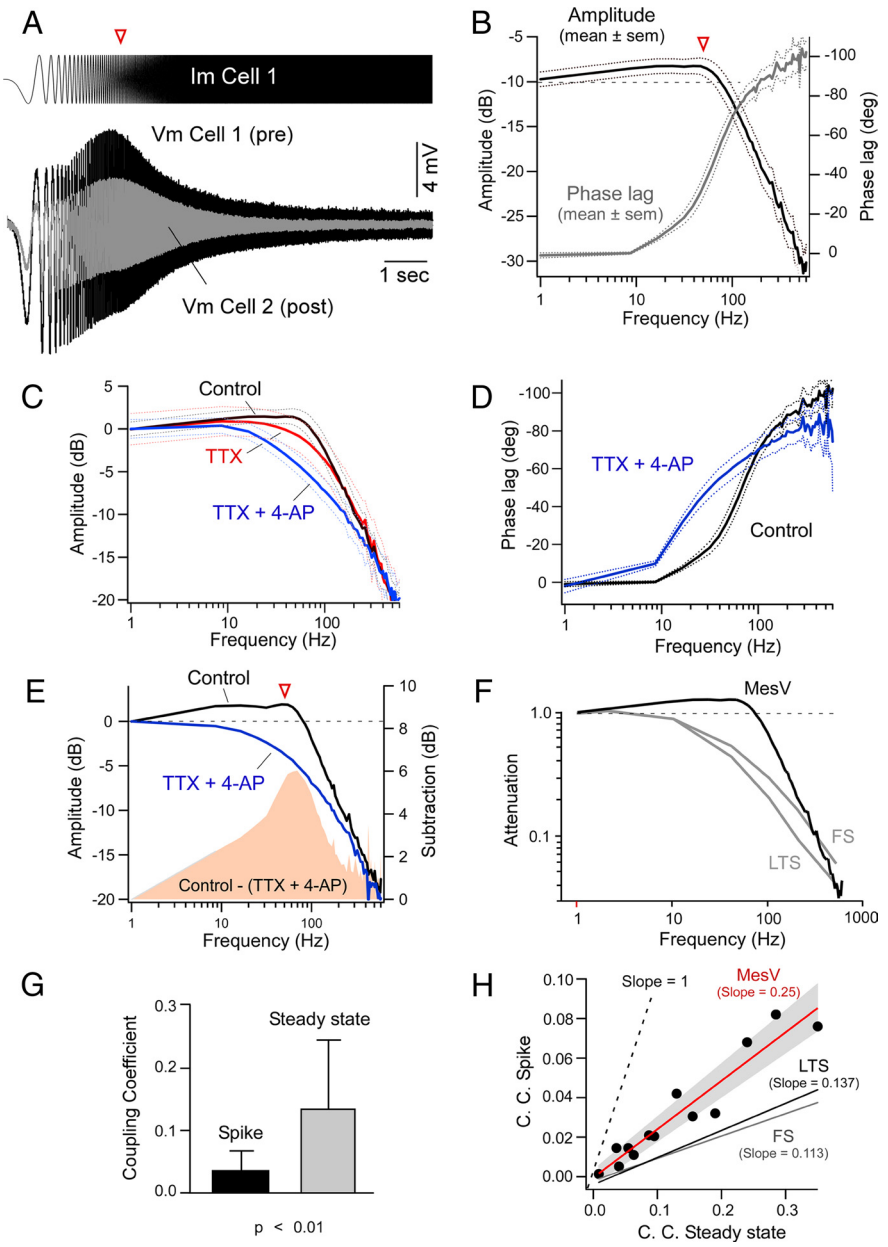

Figure 8. Intrinsic membrane properties selectively enhance the transfer of relatively high-frequency signals. ***A***, Injection of frequency modulated (2–600 Hz) sine wave current (ZAP protocol, 200 pA peak to peak) into one of the coupled cells (Im Cell 1, Pre) evokes a voltage response characterized by an increase in amplitude within a narrow frequency window (Vm Cell 1), and a parallel membrane response in a coupled cell (Vm Cell 2, Post) (bottom panel). ***B***, Average amplitude and phase of electrical coupling versus frequency between pairs of MesV neurons ($n = 8$). The amplitude and phase of the frequency-transfer characteristics were calculated as the ratio of the FFT of the postsynaptic cell over the FFT of the presynaptic cell; the dotted lines here and in ***C*** and ***D*** indicate SEM. Note that the magnitude of the transfer for frequencies ~50 Hz (arrowhead) is larger than obtained for DC (horizontal dashed line). ***C***, Magnitude of the transfer in control conditions ($n = 8$), in the presence of TTX (0.5 μM) ($n = 7$), and in the presence of both TTX and 4-AP (1 mM) ($n = 7$). The traces are represented normalized to control and were aligned at 0 dB. ***D***, Average phase of the transfer in control conditions ($n = 8$) and after the addition of a combination of TTX and 4-AP ($n = 7$). ***E***, Magnitude of the transfer for a representative case under control conditions and after the addition of TTX and 4-AP. The solid pink area represents the difference in transfer in the two conditions, illustrating the contribution of active mechanisms for frequency-transfer characteristics, particularly at ~50 Hz (arrowhead). The traces were normalized to control and aligned at 0 dB. ***F***, Average transfer between MesV neurons superimposed with those reported for electrical contacts between FS and LTS neocortical interneurons (Gibson et al., 2005). The dashed line indicates the magnitude at DC. ***G***, Difference in amplitude of coupling coefficients for presynaptic action potentials (Spike) and at steady state using long-lasting current pulses in the same group of electrically coupled MesV neurons ($n = 13$; $p < 0.01$; error bars indicate SD). ***H***, Coupling coefficient for presynaptic spikes versus the steady-state coupling coefficient in pairs of MesV neurons ($n = 13$). Data were fitted with a straight-line function (red line). The gray solid area represents SD. Similar estimates reported for FS and LTS are illustrated (Gibson et al., 2005). Spike transmission is more efficient at MesV neuron contacts, consistent with their enhanced high-frequency filtering properties. The dashed line indicates slope = 1, a condition in which spikes and DC signals would be transmitted with the same efficiency.

threshold-spiking (LTS) inhibitory interneurons (Fig. 8*F*), whose frequency-transfer characteristics were found to be consistent with a "low-pass" filter, implying entirely passive signal transmission (Gibson et al., 2005).

The voltage-dependent amplification of coupling and frequency-transfer properties of these electrical contacts suggest that they might be suited for the transfer of action potentials, which are triggered in response to sensory stimuli and thus most probably constitute the main signal source for coupling between these primary afferents. To test this possibility, the CC for action potentials was examined and determined to be on average 0.032 ± 0.027 (SD), whereas the CC obtained with hyperpolarizing pulses at steady state in the same pairs of coupled MesV neurons averaged 0.13 ± 0.11 (SD) ($p < 0.01$; $n = 13$) (Fig. 8*G*). These findings indicate that high-frequency signals like action potentials are more dramatically attenuated than DC signals, consistent with the "low-pass" properties of electrical contacts in which high-frequency signals are filtered out by the passive properties of the postsynaptic cell (Bennett, 1966; Connors and Long, 2004). However, the slope of the relationship between the CCs for action potential and steady state in the same pairs (an indication of the degree to which action potentials are attenuated compared with DC signals) was 0.25, higher than those reported for FS (0.113) and LTS (0.137) neocortical interneurons (Fig. 8*H*), whose frequency-transfer properties are purely determined by the passive properties of these cells (Gibson et al., 2005). These results support the notion of a critical role of active conductances in the transfer of high-frequency signals between MesV neurons.

Functional impact of electrical coupling between pairs of MesV neurons

Our data so far indicate that coupling in the MesV nucleus can be very strong and interacts with active conductances to improve transmission of action potentials. To investigate the functional impact of this coupling, we tested the extent to which presynaptic firing activity can influence the activity of the postsynaptic cell. As illustrated in Figure 9*A*, depolarization of a presynaptic cell with DC current evoked trains of action potentials (most MesV neurons were found to be inactive in these slices), which in turn led to synchronized firing of the previously inactive postsynaptic cell. The discharges in the postsynaptic cell originated from spikelets (Fig. 9*B*) and were temporally

correlated with the discharges of the presynaptic cell. Cross-correlation analysis exhibited a single peak of large magnitude [0.76 ± 0.25 (SD); $n = 5$] and brief delay [1.48 ± 1.28 ms (SD); $n = 5$] (Fig. 9*D*). Moreover, the degree of synchronization expressed as the "cross-correlation function index" (see Materials and Methods) showed a positive correlation ($R^2 = 0.75$) with the coupling coefficient, indicating a strong and precise synchronization of the activity of these neurons. In contrast, and despite the presence of high-frequency firing in the recorded MesV neurons (evoked by depolarizing the recorded cells with positive DC current), no correlation was found between pairs of noncoupled cells (Fig. 9*C*,*D*), indicating that electrical coupling is required for the synchronization of the activity of these afferents. Thus, firing of a MesV neuron can lead to firing of a second coupled neuron and electrical transmission contributes to the synchronization of the activity of these afferents.

MesV neurons are sensory afferents that can be simultaneously activated by strong sensory stimuli. We therefore examined the functional consequence of electrical coupling when both coupled cells were simultaneously depolarized. For this purpose, depolarization in pairs of MesV neurons was adjusted to evoke only one or two spikes when activated in isolation (Fig. 10*A*, left and middle panels). Remarkably, coactivation of the cells with the same depolarizing currents led now to strong bursts of action potentials in both coupled cells (Fig. 10*A*, right panel). The number of spikes averaged 1.44 ± 0.12 (SEM) when cells where activated in isolation and 7.18 ± 1.12 (SEM) when coactivated ($n = 48$; $p < 0.01$) (Fig. 10*B*). This dramatic phenomenon indicates that electrical coupling strongly enhances the excitability of MesV neurons when they are simultaneously active. We reasoned that such increased excitability might result from the alleviation of "loading" from the coupled inactive cell. Loading refers to the leak of current from an active depolarized cell to an inactive hyperpolarized cell, and is known to lower the effective input resistance (R_{in}) of the coupled neurons (Getting, 1974; Bennett and Zukin, 2004). Because MesV neurons are mainly coupled in pairs, this effect could play an important functional role and be experimentally detected when manipulating the coupled cells. To assess this phenomenon, the R_{in} of each cell in pairs of coupled MesV neurons was estimated using current pulses that were applied either independently or simultaneously in both cells. The estimates of R_{in} where significantly higher when pulses were simultaneously applied, averaging 71.9 ± 28.8 MΩ (SD) and 96.8 ± 30.9 MΩ (SD) for independent and simultaneous application, respectively ($n = 9$; $p < 0.01$) (Fig. 10*C*). Supporting this observation, R_{in} was found to be significantly higher after application of the gap junction blocker MFA, averaging 145.3 ± 67.4 MΩ (SD) and 183.3 ± 81.8 MΩ (SD) in control and after MFA, respectively ($p < 0.01$, $n = 16$). [Although not significantly different, the values of R_{in} of coupled and uncoupled MesV neurons in rat slices averaged 104 ± 45.9 MΩ (SD) ($n = 82$) and 118 ± 46.8 MΩ (SD) ($n = 50$), respectively ($p = 0.09$).] As expected, the effect on R_{in} was proportional to the degree of coupling between these neurons (Fig. 10*D*). This finding indicates that "loading" likely plays an important functional role in these generally strongly coupled cells substantially dampening the R_{in} of the cell, despite the small number of neurons (two to four) forming the coupled clusters. Moreover, because in most cases coupling occurs between pairs, parallel variations in the membrane potential of these neurons will instantaneously alleviate this effect ("unloading"), increasing the excitability of the coupled neurons.

While useful in exposing the contribution of "loading" to the excitability of MesV neurons, depolarizations evoked with long current pulses hardly resemble physiological conditions. However, the characteristic subthreshold membrane potential oscillations of ~50–100 Hz could provide the required sustained

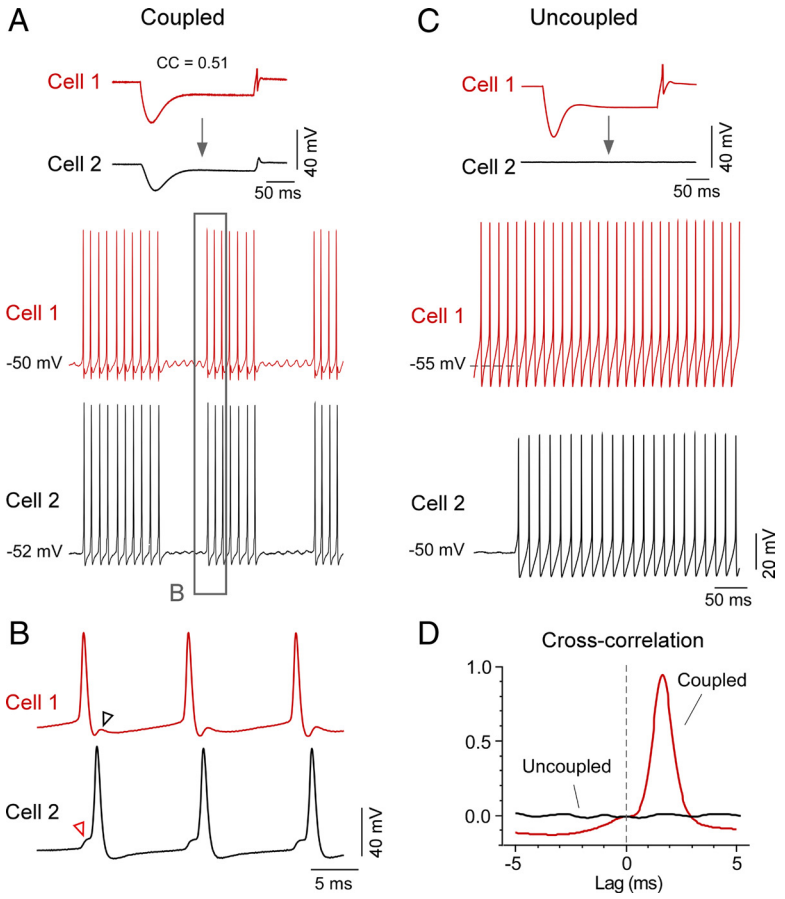

Figure 9. Gap junctions promote robust synchronization of spikes between MesV neurons. ***A***, Simultaneous recordings from a pair of strongly coupled MesV neurons (CC = 0.51) (top panel). Cell 1 was slightly depolarized using DC current (40 pA), which elicited in both cells episodes of subthreshold oscillations of their membrane potentials and synchronous bursts of action potentials. ***B***, The boxed area in ***A*** is illustrated at an expanded temporal scale. In this example, cell 1 acts as the command cell and cell 2 as its follower. Note that the discharge of a spike in cell 1 elicits a spikelet in cell 2 (red arrowhead) from which the spike initiates. Reciprocally, the spike in cell 2 elicits a spikelet in cell 1 (black arrowhead), which coincides with the AHP and likely the refractory period of this cell. ***C***, Simultaneous recordings from a pair of uncoupled MesV neurons. In this example, cell 1 was spontaneously active and cell 2 was slightly depolarized using DC current injection to induce firing activity. ***D***, Cross-correlation analysis between cells of the pairs of MesV neurons depicted in ***A*** and ***C***. Cross-correlograms are shown superimposed and indicate a high degree of synchronization between spikes of the coupled cells. In contrast, despite their high-frequency firing, the uncoupled pair did not show synchronization. Note the high precision (lag, <2 ms) and strength (cross-correlation function index of ~1) of the synchronization between the activities of the coupled cells.

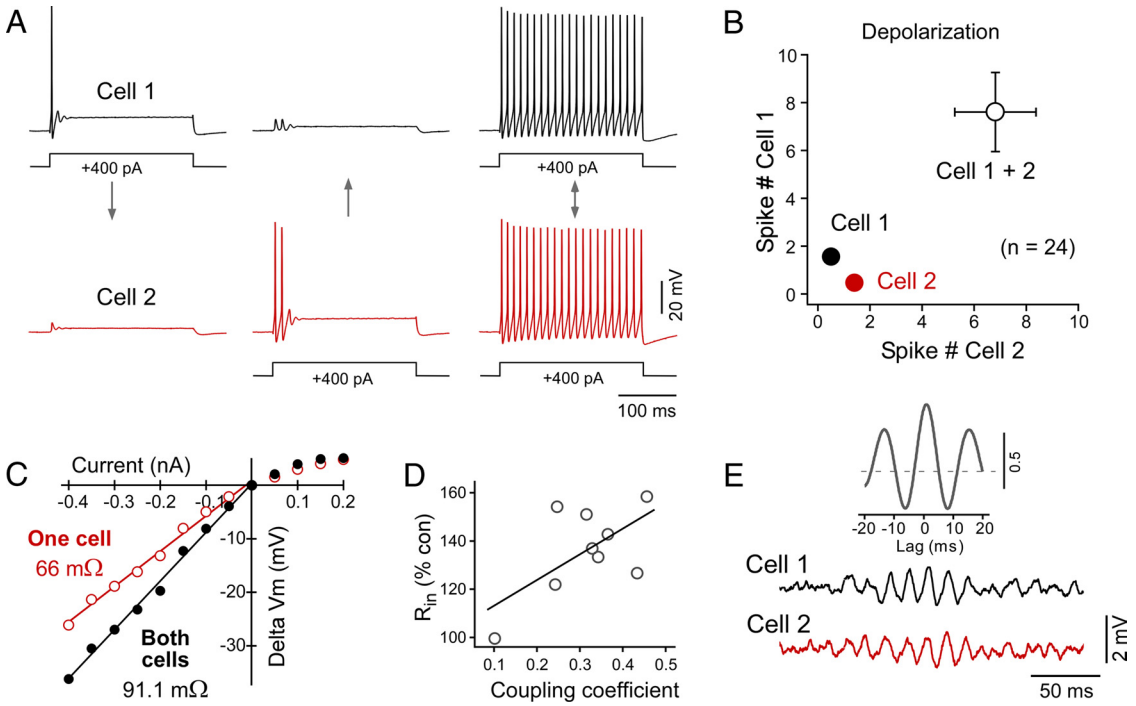

Figure 10. Functional impact of electrical coupling between pairs of MesV neurons. ***A***, Coincidence detection between a pair of MesV neurons. Injection of a depolarizing current pulse in cell 1 or cell 2 induced a brief firing response consisting of one or two spikes at the beginning of the current step, with their corresponding coupling potentials (spikelet) in the coupled cell (left and middle traces). Simultaneous activation of these two neurons with the current pulses of the same magnitude (right traces) evoked instead a robust repetitive discharge at each cell, consisting of 20 action potentials. ***B***, Effect of simultaneous depolarization in electrically coupled pairs of MesV neurons. Average number of spikes in cell 1 (ordinate) are plotted against spikes in cell 2 (abscissa) under the following conditions: current pulse was applied to cell 1 (black circle), applied to cell 2 (red circle) and applied simultaneously to both cells (open circle). Error bars represent SEM; bars are smaller than symbol for individual depolarizations. ***C***, Simultaneous depolarization enhances input resistance by canceling the leaking or "loading" of currents to an inactive coupled neuron. Membrane voltage (ΔV_m, ordinates) versus current (abscissa) relationships obtained in one of a pair of electrically coupled MesV neurons in two conditions: current pulses applied to one cell (red open circles) or simultaneously to both cells (black circles). Because both input resistances were comparable, the cells were isopotential. The estimated input resistance was 38% higher when both cells were depolarized (66 MΩ, single cell, vs 91.1 MΩ, both cells). ***D***, Increase in input resistance obtained for eight pairs of electrically coupled MesV neurons as a function of their CC, when both cells were simultaneously depolarized. Input resistance is expressed as a percentage of the value obtained when cells were independently depolarized. The effect is proportionally larger in highly coupled pairs. Data were obtained from one of the cells of each tested pair and fitted to a straight-line function. ***E***, Synchrony of voltage membrane oscillations in pairs of electrically coupled MesV neurons. Spontaneous oscillations (bottom panel), triggered by slightly depolarizing both cells with DC current (50–100 pA) in this example, were highly synchronized as indicated by cross-correlation analysis (top panel).

depolarization (Pedroarena et al., 1999). To investigate whether these oscillations become synchronized, we recorded from pairs of electrically coupled MesV neurons that were injected with just enough depolarizing current to generate membrane potential oscillations (Fig. 10*E*) ($n = 4$). As illustrated in the inset of Figure 10*E*, these oscillations quickly became synchronized, supporting the idea that simultaneous and symmetrical fluctuations of membrane potential, which alleviate "loading," can occur under physiological conditions between pairs of MesV neurons. Consistent with this possibility, MesV neurons are known to receive excitatory synaptic inputs from several brainstem nuclei (including the supratrigeminal area), which were shown to be strong enough to initiate subthreshold oscillations and spiking (Verdier et al., 2004). Divergent presynaptic inputs from these structures could lead to simultaneous depolarization of MesV neurons. Thus, electrical coupling between pairs of MesV neurons act as a coincidence detector and, by reducing "loading," increases the effective R_{in} of the coupled cells that in turn allows subthreshold Na^+ currents to operate under more efficient conditions, leading to synchronized firing (Fig. 11*A*).

Discussion

We describe the properties of electrical coupling between neurons of the rodent MesV nucleus, including the identification of its molecular determinants and characterization of its biophysical properties and network organization. This work builds on seminal reports on the MesV nucleus that provided initial evidence for the existence of electrical coupling in the mammalian brain (Hinrichsen, 1970; Hinrichsen and Larramendi, 1970; Baker and Llinás, 1971).

Coupling occurs at somatic contacts containing Cx36

Our results indicate that Cx36 is heavily concentrated at identifiable MesV somato-somatic contacts in both rat and mouse brain. This connexin has been localized ultrastructurally to gap junctions in mammalian brain, and Cx36-mediated electrical transmission has been demonstrated in numerous brain areas (Bennett and Zukin, 2004; Hormuzdi et al., 2004; Meier and Dermietzel, 2006; Rash et al., 2007a,b). Our immunofluorescence detection of Cx36 with the fidelity and resolution afforded by current imaging techniques now provides unambiguous evidence for sites that enable electrical coupling between MesV neurons, producing results consistent with early ultrastructural observations of gap junction-like structures at MesV somatic appositions and with the proposal that coupling likely occurs at these large areas of apposition (Hinrichsen and Larramendi, 1970).

The presence of tracer and electrical coupling we found between MesV neurons in Cx36 KO mice parallels observations of a similar persistence of low-level coupling in the reticular thalamic

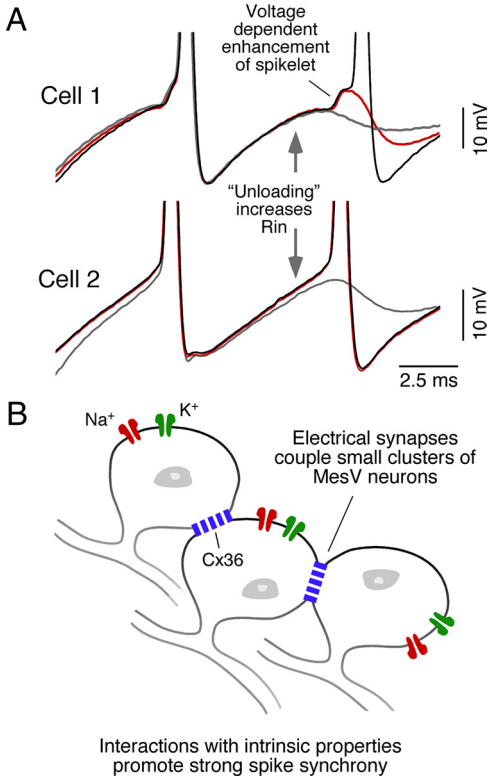

Figure 11. Synergy between electrical coupling and intrinsic membrane properties promotes synchrony of repetitive discharges between pairs of MesV neurons. ***A***, Superimposed traces were obtained between a pair of electrically coupled MesV neurons, to illustrate the mechanisms that lead to synchronization of firing activity. Voltage-dependent resonant membrane properties enhance the transfer of signals within a range of frequencies that facilitate action potential initiation. Strong electrical coupling between pairs of MesV neurons act as a coincidence detector (gray trace) that, by reducing loading, increases the effective R_{in} that in turn allows subthreshold Na^+ currents to operate under more efficient conditions enhancing "spikelets" (red trace), leading to synchronized firing of the coupled cells (black trace). ***B***, The MesV is organized in small groups of electrically coupled neurons. The interaction of electrical coupling with intrinsic membrane properties (Na^+, K^+ conductances) promotes robust and synchronous repetitive discharges that are likely to enhance the synaptic influence of pairs or small clusters of sensory afferents on postsynaptic cells.

nucleus of these mice (Lee et al., 2010), presumably mediated by gap junctions formed by another connexin. It is unclear whether this putative additional connexin normally occurs along with Cx36 at MesV neuronal contacts or, alternatively, represents the upregulation of a new connexin in Cx36 KO mice. Our attempts to identify this connexin so far have excluded many of the known connexins, none of which display anywhere near the high density of immunolabeling seen for Cx36 at MesV neuronal appositions (see Results).

A small fraction of channels is responsible for electrical coupling

Taking advantage of current electrophysiological approaches, our recordings from pairs of MesV neurons provide direct evidence for the existence of electrical coupling between these cells. We found that electrical coupling could be very strong and exhibited symmetrical and largely nonrectifying properties (although the existence of weak rectification cannot be ruled out). This coupling is supported by a small number of functional channels (~200), which represent a very small proportion of the gap junction channels estimated to be present at the contacts (~0.1%). These calculations were enabled by unprecedented experimental access to these electrical synapses, at least in mammalian systems, which allowed estimation of the average number of open channels mediating electrical coupling. The fraction of open channels was similar for independent estimates of junctional conductance, that is, using either indirect (from measurements of CC and R_{in}) or direct (voltage-clamp) approaches. However, these estimates assume a unitary conductance of Cx36 channels, which has been similarly reported by various groups (Srinivas et al., 1999b; Teubner et al., 2000), but which has not been so far validated in a native neuronal gap junction. The small proportion of open channels found is consistent with similar estimates obtained at mixed synapses formed by afferent terminals on the goldfish Mauthner cell, where only a small percentage of channels (~1%) supports the electrical component of a unitary mixed synaptic potential (Lin and Faber, 1988) and where the number of channels was obtained from direct ultrastructural reconstruction of these terminals (Tuttle et al., 1986). Furthermore, a similar fraction of open Cx36 gap junction channels (~0.1%) was obtained in expression systems combining electrophysiological and imaging approaches (F. Bukauskas, personal communication). Despite our use of indirect methods, this agreement between the present results and those derived from other approaches in Mauthner cells and transfected cells is noteworthy and suggests that our estimates of channel number were not significantly affected by our assumptions. Thus, although surprisingly small, our estimates are likely to reflect an important functional property of electrical synapses. From the functional point of view, it has been suggested (Flores et al., 2012) that the excess of nonconducting channels might serve as adhesion molecules (Elias et al., 2007; Derangeon at al., 2009), providing mechanical stability for those open channels responsible for coupling.

Electrical coupling in the MesV nucleus is organized in small clusters of neurons

It was suggested that, as a consequence of electrical coupling, the MesV nucleus could act as a functional unit during jaw reflexes (Hinrichsen, 1970; Lazarov, 2007). While this idea implies coupling of large neuronal ensembles, early *in vivo* evidence supported the notion that coupling in the MesV nucleus could be organized in small groups of neurons (Baker and Llinás, 1971). Our data indicate that MesV neurons are indeed primarily coupled in pairs or small clusters: (1) tracer-coupling analysis showed that a large proportion of MesV neurons were coupled in pairs and, in much less proportion, triplets or quadruplets; (2) analysis of Cx36 labeling was consistent with tracer-coupling results, showing that MesV somata engage in Cx36-containing contacts most often with one other MesV somata; and (3) despite the massive overall reduction in coupling in Cx36 KO mice, the incidence of coupled pairs, triplets, and quadruplets remained similar to that observed in WT mice. These findings are consistent with a more recent report in which tracer coupling was observed between pairs of MesV neurons (Verdier et al., 2004). Thus, from the perspective of the deployment of electrical synapses, the MesV nucleus seems to be functionally organized in pairs or small clusters of coupled neurons.

Some MesV neurons were found not to be coupled despite displaying labeling for Cx36 at areas of apposition between neighboring somata, suggesting that coupling between these neurons could be under regulatory control. Indeed, Cx36 has been shown to be a target of modulation by various intracellular regulatory systems (Urschel et al., 2006; Kothmann et al., 2007, 2009; Alev et al., 2008). Moreover, MesV somata receive abundant syn-

aptic inputs from various brainstem structures (Luo and Li, 1991; Bae et al., 1996; Kishimoto et al., 1998; Lazarov, 2002; Pose et al., 2003) and these inputs contain neurotransmitters that have been reported to regulate electrical coupling in other systems (Pereda et al., 1992, 1998; Onn and Grace, 1994; Rörig and Sutor, 1996; Landisman and Connors, 2005; Urschel at al., 2006; Kothmann et al., 2009).

Interaction of coupling with intrinsic properties lead to synchronized firing

We show here that electrical synapses between MesV neurons exhibit properties seemingly optimized for transfer of the upstroke of action potentials and the precise synchronization of pairs (or very small clusters) of neurons. This is unlike most examples of electrical synapses reported so far, which behave as simple "low-pass" filters (Veruki and Hartveit, 2002; Connors and Long, 2004). The frequency transfer at MesV electrical synapses is enhanced within a band of frequencies that peaks at ~50 Hz. Strikingly, as a result of this property, the CC at the peak frequency is higher than that obtained at steady state (DC). This frequency preference is a consequence of the electrophysiological properties of MesV neurons, which exhibit membrane resonant properties with a ~50 (24–90) Hz peak (Wu et al., 2001, 2005). Consistent with this interpretation, the enhanced transfer of high-frequency signals was prevented by a combination of TTX, which blocks Na^+ currents, and 4-AP, which blocks low-threshold K^+ currents among others. Persistent Na^+ currents and subthreshold K^+ currents such as the I_A are known to promote resonant behavior in neurons (Hutcheon and Yarom, 2000; Izhikevich, 2007), and both of these currents are prominent in MesV neurons (Del Negro and Chandler, 1997; Wu et al., 2001, 2005; Hsiao et al., 2009). Consequently, coupling of action potentials between MesV neurons is comparatively stronger than found among electrically coupled neocortical inhibitory interneurons, whose frequency transfer obeys entirely the passive properties of these cells (Gibson et al., 2005). Equally relevant, active conductances mitigated phase lag, thus contributing to spike synchrony. Additionally, as reported for other cell types (Mann-Metzer and Yarom, 1999; Curti and Pereda, 2004; Dugué et al., 2009), the persistent Na^+ current endowed electrical coupling with voltage-dependent amplification, further emphasizing the role of active conductances in improving the efficacy of electrical coupling between MesV neurons.

We also show here that coupling between MesV neurons, as proposed in the retina (Veruki and Hartveit, 2002) and neocortex (Galarreta and Hestrin, 1999), acts as a "coincidence detector" (Veruki and Hartveit, 2002) sensing the temporal coincidence of depolarizations, which by alleviating "loading" (the leak of currents to coupled inactive cells) increases the apparent R_{in} of the coupled cells (Getting, 1974; Getting and Willows, 1974). The increased R_{in} enhances the coupling potential, which in turn activates a larger fraction of persistent Na^+ channels, resulting in further enhancement of coupling and increased probability of synchronized firing (Fig. 11). Thus, the interaction between electrical coupling and intrinsic membrane properties enhances the transfer of action potentials between somata of MesV neurons, leading to a strong synchronization of the coupled sensory afferents.

Coupling between MesV neurons develops with age

Electrical synapses are widespread during development, in which they usually precede the formation of chemical synapses (Connors et al., 1983; Lo Turco and Kriegstein, 1991; Peinado et al., 1993). In the mammalian brain, electrical synapses are developmentally regulated, being prevalent at early developmental stages, decreasing with age, and persisting in lower abundance in various cell types and structures in adult brain. Our analysis of tracer coupling and immunochemical detection of Cx36 indicate that, in contrast to this common rule, electrical coupling between MesV neurons is absent during early developmental stages and appears at P8 to remain throughout adulthood, with similar incidence. This sudden emergence of coupling parallels the development of intrinsic membrane properties that support repetitive firing of these neurons. Coincidently, the feeding motor patterns in the rat gradually evolve from sucking to chewing at approximately P12 (Westneat and Hall, 1992), when both electrical coupling and bursting are fully established in the MesV nucleus. Thus, rather than a developmental feature, electrical synapses constitute an essential characteristic of the adult cellular phenotype of neurons in the MesV nucleus.

Functional considerations

MesV neurons are the somata of primary sensory afferents that originate in spindles of jaw-closing muscles (masseter) and mechanoreceptors of periodontal ligaments and that contribute to masticatory behaviors (Kolta et al., 1990; Westberg et al., 2000). It has been proposed that MesV afferents might be compartmentalized (i.e., the peripheral and central ends of these afferents could under certain conditions function independently) (Westberg et al., 2000). By virtue of the presence of electrical synapses, the somata of these afferents representing the central compartment are likely to play an integrative role promoting the synchronization of coupled afferents. It has been suggested that this enhances or "amplifies" the influence of active sensory afferents on postsynaptic jaw-closing motoneurons (Verdier et al., 2004). Our results are consistent with such a functional role; the synergic interaction between electrical coupling and intrinsic membrane properties promotes a strong synchronization and increases the excitability of coupled afferents, providing the underlying cellular mechanisms for the proposed "amplification" of sensory input.

References

Alev C, Urschel S, Sonntag S, Zoidl G, Fort AG, Höher T, Matsubara M, Willecke K, Spray DC, Dermietzel R (2008) The neuronal connexin36 interacts with and is phosphorylated by CaMKII in a way similar to CaMKII interaction with glutamate receptors. Proc Natl Acad Sci U S A 105:20964–20969.

Bae YC, Nakagawa S, Yasuda K, Yabuta NH, Yoshida A, Pil PK, Moritani M, Chen K, Nagase Y, Takemura M, Shigenaga Y (1996) Electron microscopic observation of synaptic connections of jaw-muscle spindle and periodontal afferent terminals in the trigeminal motor and supratrigeminal nuclei in the cat. J Comp Neurol 374:421–435.

Baker R, Llinás R (1971) Electrotonic coupling between neurones in the rat mesencephalic nucleus. J Physiol 212:45–63.

Bennett MV (1966) Physiology of electrotonic junctions. Ann N Y Acad Sci 137:509–539.

Bennett MV (1997) Gap junctions as electrical synapses. J Neurocytol 26:349–366.

Bennett MV, Zukin RS (2004) Electrical coupling and neuronal synchronization in the Mammalian brain. Neuron 41:495–511.

Ciolofan C, Lynn BD, Wellershaus K, Willecke K, Nagy JI (2007) Spatial relationships of connexin36, connexin57 and zonula occludens-1 (ZO-1) in the outer plexiform layer of mouse retina. Neuroscience 148:473–488.

Condorelli DF, Parenti R, Spinella F, Trovato Salinaro A, Belluardo N, Cardile V, Cicirata F (1998) Cloning of a new gap junction gene (Cx36) highly expressed in mammalian brain neurons. Eur J Neurosci 10:1202–1208.

Connors BW, Long MA (2004) Electrical synapses in the mammalian brain. Annu Rev Neurosci 27:393–418.

Connors BW, Benardo LS, Prince DA (1983) Coupling between neurons of the developing rat neocortex. J Neurosci 3:773–782.
Curti S, Pereda AE (2004) Voltage-dependent enhancement of electrical coupling by a subthreshold sodium current. J Neurosci 24:3999–4010.
Curti S, Gómez L, Budelli R, Pereda AE (2008) Subthreshold sodium current underlies essential functional specializations at primary auditory afferents. J Neurophysiol 99:1683–1699.
Deans MR, Gibson JR, Sellitto C, Connors BW, Paul DL (2001) Synchronous activity of inhibitory networks in neocortex requires electrical synapses containing connexin36. Neuron 31:477–485.
Del Negro CA, Chandler SH (1997) Physiological and theoretical analysis of K^+ currents controlling discharge in neonatal rat mesencephalic trigeminal neurons. J Neurophysiol 77:537–553.
Derangeon M, Spray DC, Bourmeyster N, Sarrouilhe D, Hervé JC (2009) Reciprocal influence of connexins and apical junction proteins on their expressions and functions. Biochim Biophys Acta 1788:768–778.
Dessem D, Taylor A (1989) Morphology of jaw-muscle spindle afferents in the rat. J Comp Neurol 282:389–403.
Devor A, Yarom Y (2002) Electrotonic coupling in the inferior olivary nucleus revealed by simultaneous double patch recordings. J Neurophysiol 87:3048–3058.
Dugué GP, Brunel N, Hakim V, Schwartz E, Chat M, Lévesque M, Courtemanche R, Léna C, Dieudonné S (2009) Electrical coupling mediates tunable low-frequency oscillations and resonance in the cerebellar Golgi cell network. Neuron 61:126–139.
Elias LA, Wang DD, Kriegstein AR (2007) Gap junction adhesion is necessary for radial migration in the neocortex. Nature 448:901–907.
Flores C, Nannapaneni S, Davidson K, Yasumura T, Bennett MV, Rash JR, Pereda A (2012) Trafficking of gap junction channels at a vertebrate electrical synapse in vivo. Advance online publication. Retrieved February 16, 2012. doi:10.1073/pnas.1121557109.
Galarreta M, Hestrin S (1999) A network of fast-spiking cells in the neocortex connected by electrical synapses. Nature 402:72–75.
Getting PA (1974) Modification of neuron properties by electrotonic synapses. I. Input resistance, time constant, and integration. J Neurophysiol 37:846–857.
Getting PA, Willows AO (1974) Modification of neuron properties by electrotonic synapses. II. Burst formation by electrotonic synapses. J Neurophysiol 37:858–868.
Gibson JR, Beierlein M, Connors BW (2005) Functional properties of electrical synapses between inhibitory interneurons of neocortical layer 4. J Neurophysiol 93:467–480.
Hinrichsen CF (1970) Coupling between cells of the trigeminal mesencephalic nucleus. J Dent Res 49 [Suppl]:1369–1373.
Hinrichsen CF, Larramendi LM (1970) The trigeminal mesencephalic nucleus. II. Electron microscopy. Am J Anat 127:303–319.
Hormuzdi SG, Filippov MA, Mitropoulou G, Monyer H, Bruzzone R (2004) Electrical synapses: a dynamic signaling system that shapes the activity of neuronal networks. Biochim Biophys Acta 1662:113–137.
Hsiao CF, Kaur G, Vong A, Bawa H, Chandler SH (2009) Participation of Kv1 channels in control of membrane excitability and burst generation in mesencephalic V neurons. J Neurophysiol 101:1407–1418.
Hutcheon B, Yarom Y (2000) Resonance, oscillation and the intrinsic frequency preferences of neurons. Trends Neurosci 23:216–222.
Izhikevich EM (2007) Dynamical systems in neuroscience: the geometry of excitability and bursting. Cambridge, MA: MIT.
Kamasawa N, Furman CS, Davidson KG, Sampson JA, Magnie AR, Gebhardt BR, Kamasawa M, Yasumura T, Zumbrunnen JR, Pickard GE, Nagy JI, Rash JE (2006) Abundance and ultrastructural diversity of neuronal gap junctions in the OFF and ON sublaminae of the inner plexiform layer of rat and mouse retina. Neuroscience 142:1093–1117.
Khakh BS, Henderson G (1998) Hyperpolarization-activated cationic currents (I_h) in neurones of the trigeminal mesencephalic nucleus of the rat. J Physiol 510:695–704.
Kishimoto H, Bae YC, Yoshida A, Moritani M, Takemura M, Nakagawa S, Nagase Y, Wada T, Sessle BJ, Shigenaga Y (1998) Central distribution of synaptic contacts of primary and secondary jaw muscle spindle afferents in the trigeminal motor nucleus of the cat. J Comp Neurol 391:50–63.
Kolta A, Lund JP, Rossignol S (1990) Modulation of activity of spindle afferents recorded in trigeminal mesencephalic nucleus of rabbit during fictive mastication. J Neurophysiol 64:1067–1076.
Kothmann WW, Li X, Burr GS, O'Brien J (2007) Connexin 35/36 is phosphorylated at regulatory sites in the retina. Vis Neurosci 24:363–375.
Kothmann WW, Massey SC, O'Brien J (2009) Dopamine-stimulated dephosphorylation of connexin 36 mediates AII amacrine cell uncoupling. J Neurosci 29:14903–14911.
Landisman CE, Connors BW (2005) Long-term modulation of electrical synapses in the mammalian thalamus. Science 310:1809–1813.
Lazarov NE (2002) Comparative analysis of the chemical neuroanatomy of the mammalian trigeminal ganglion and mesencephalic trigeminal nucleus. Prog Neurobiol 66:19–59.
Lazarov NE (2007) Neurobiology of orofacial proprioception. Brain Res Rev 56:362–383.
Lee SC, Cruikshank SJ, Connors BW (2010) Electrical and chemical synapses between relay neurons in developing thalamus. J Physiol 588:2403–2415.
Li X, Olson C, Lu S, Kamasawa N, Yasumura T, Rash JE, Nagy JI (2004) Neuronal connexin36 association with zonula occludens-1 protein (ZO-1) in mouse brain and interaction with the first PDZ domain of ZO-1. Eur J Neurosci 19:2132–2146.
Li X, Kamasawa N, Ciolofan C, Olson CO, Lu S, Davidson KG, Yasumura T, Shigemoto R, Rash JE, Nagy JI (2008a) Connexin45-containing neuronal gap junctions in rodent retina also contain connexin36 in both apposing hemiplaques, forming bi-homotypic gap junctions, with scaffolding contributed by zonula occludens-1. J Neurosci 28:9769–9789.
Li X, Penes M, Odermatt B, Willecke K, Nagy JI (2008b) Ablation of Cx47 in transgenic mice leads to the loss of MUPP1, ZONAB and multiple connexins at oligodendrocyte-astrocyte gap junctions. Eur J Neurosci 28:1503–1517.
Liem RS, Copray JC, van Willigen JD (1991) Ultrastructure of the rat mesencephalic trigeminal nucleus. Acta Anat (Basel) 140:112–119.
Lin JW, Faber DS (1988) Synaptic transmission mediated by single club endings on the goldfish Mauthner cell. I. Characteristics of electrotonic and chemical postsynaptic potentials. J Neurosci 8:1302–1312.
Llinás R (1975) Electrical synaptic transmission in the mammalian central nervous system. In: Golgi Centennial Symposium: proceedings (Santini M, ed), pp 379–386. New York: Raven.
Lo Turco JJ, Kriegstein AR (1991) Clusters of coupled neuroblasts in embryonic neocortex. Science 252:563–566.
Luo PF, Li JS (1991) Monosynaptic connections between neurons of trigeminal mesencephalic nucleus and jaw-closing motoneurons in the rat: an intracellular horseradish peroxidase labelling study. Brain Res 559:267–275.
Lynn BD, Tress O, May D, Willecke K, Nagy JI (2011) Ablation of connexin30 in transgenic mice alters expression patterns of connexin26 and connexin32 in glial cells and leptomeninges. Eur J Neurosci 34:1783–1793.
Mann-Metzer P, Yarom Y (1999) Electrotonic coupling interacts with intrinsic properties to generate synchronized activity in cerebellar networks of inhibitory interneurons. J Neurosci 19:3298–3306.
Meier C, Dermietzel R (2006) Electrical synapses—gap junctions in the brain. Results Probl Cell Differ 43:99–128.
Mills SL, Massey SC (1995) Differential properties of two gap junctional pathways made by AII amacrine cells. Nature 377:734–737.
Nagy JI, Buss M, Daddona PE (1986) On the innervation of trigeminal mesencephalic primary afferent neurons by adenosine deaminase-containing projections from the hypothalamus in the rat. Neuroscience 17:141–156.
Nagy JI, Ionescu AV, Lynn BD, Rash JE (2003) Coupling of astrocyte connexins Cx26, Cx30, Cx43 to oligodendrocyte Cx29, Cx32, Cx47; implications from normal and connexin32 knockout mice. Glia 44:205–218.
Nagy JI, Dudek FE, Rash JE (2004) Update on connexins and gap junctions in neurons and glia in the mammalian nervous system. Brain Res Rev 47:191–215.
Nagy JI, Lynn BD, Tress O, Willecke K, Rash JE (2011) Connexin26 expression in brain parenchymal cells demonstrated by targeted connexin ablation in transgenic mice. Eur J Neurosci 34:263–271.
Onn SP, Grace AA (1994) Dye coupling between rat striatal neurons recorded in vivo: compartmental organization and modulation by dopamine. J Neurophysiol 71:1917–1934.
Pan F, Mills SL, Massey SC (2007) Screening of gap junction antagonists on dye coupling in the rabbit retina. Vis Neurosci 24:609–618.
Parker PR, Cruikshank SJ, Connors BW (2009) Stability of electrical coupling despite massive developmental changes of intrinsic neuronal physiology. J Neurosci 29:9761–9770.

Pedroarena CM, Pose IE, Yamuy J, Chase MH, Morales FR (1999) Oscillatory membrane potential activity in the soma of a primary afferent neuron. J Neurophysiol 82:1465–1476.

Peinado A, Yuste R, Katz LC (1993) Gap junctional communication and the development of local circuits in neocortex. Cereb Cortex 3:488–498.

Pereda A, Triller A, Korn H, Faber DS (1992) Dopamine enhances both electrotonic coupling and chemical excitatory postsynaptic potentials at mixed synapses. Proc Natl Acad Sci U S A 89:12088–12092.

Pereda AE, Bell TD, Chang BH, Czernik AJ, Nairn AC, Soderling TR, Faber DS (1998) Ca^{2+}/calmodulin-dependent kinase II mediates simultaneous enhancement of gap-junctional conductance and glutamatergic transmission. Proc Natl Acad Sci U S A 95:13272–13277.

Pose I, Sampogna S, Chase MH, Morales FR (2003) Mesencephalic trigeminal neurons are innervated by nitric oxide synthase-containing fibers and respond to nitric oxide. Brain Res 960:81–89.

Rash JE, Yasumura T, Dudek FE, Nagy JI (2001) Cell-specific expression of connexins and evidence of restricted gap junctional coupling between glial cells and between neurons. J Neurosci 21:1983–2000.

Rash JE, Olson CO, Davidson KG, Yasumura T, Kamasawa N, Nagy JI (2007a) Identification of connexin36 in gap junctions between neurons in rodent locus coeruleus. Neuroscience 147:938–956.

Rash JE, Olson CO, Pouliot WA, Davidson KG, Yasumura T, Furman CS, Royer S, Kamasawa N, Nagy JI, Dudek FE (2007b) Connexin36 vs. connexin32, "miniature" neuronal gap junctions, and limited electrotonic coupling in rodent suprachiasmatic nucleus. Neuroscience 149:350–371.

Rörig B, Sutor B (1996) Serotonin regulates gap junction coupling in the developing rat somatosensory cortex. Eur J Neurosci 8:1685–1695.

Söhl G, Degen J, Teubner B, Willecke K (1998) The murine gap junction gene connexin36 is highly expressed in mouse retina and regulated during brain development. FEBS Lett 428:27–31.

Srinivas M, Costa M, Gao Y, Fort A, Fishman GI, Spray DC (1999a) Voltage dependence of macroscopic and unitary currents of gap junction channels formed by mouse connexin50 expressed in rat neuroblastoma cells. J Physiol 517:673–689.

Srinivas M, Rozental R, Kojima T, Dermietzel R, Mehler M, Condorelli DF, Kessler JA, Spray DC (1999b) Functional properties of channels formed by the neuronal gap junction protein connexin36. J Neurosci 19:9848–9855.

Teubner B, Degen J, Söhl G, Güldenagel M, Bukauskas FF, Trexler EB, Verselis VK, De Zeeuw CI, Lee CG, Kozak CA, Petrasch-Parwez E, Dermietzel R, Willecke K (2000) Functional expression of the murine connexin 36 gene coding for a neuron-specific gap junctional protein. J Membr Biol 176:249–262.

Tuttle R, Masuko S, Nakajima Y (1986) Freeze-fracture study of the large myelinated club ending synapse on the goldfish Mauthner cell: special reference to the quantitative analysis of gap junctions. J Comp Neurol 246:202–211.

Urschel S, Höher T, Schubert T, Alev C, Söhl G, Wörsdörfer P, Asahara T, Dermietzel R, Weiler R, Willecke K (2006) Protein kinase A-mediated phosphorylation of connexin36 in mouse retina results in decreased gap junctional communication between AII amacrine cells. J Biol Chem 281:33163–33171.

Vaney DI (2002) Retinal neurons: cell types and coupled networks. Prog Brain Res 136:239–254.

Verdier D, Lund JP, Kolta A (2004) Synaptic inputs to trigeminal primary afferent neurons cause firing and modulate intrinsic oscillatory activity. J Neurophysiol 92:2444–2455.

Veruki ML, Hartveit E (2002) AII (Rod) amacrine cells form a network of electrically coupled interneurons in the mammalian retina. Neuron 33:935–946.

Veruki ML, Hartveit E (2009) Meclofenamic acid blocks electrical synapses of retinal AII amacrine and on-cone bipolar cells. J Neurophysiol 101:2339–2347.

Westberg KG, Kolta A, Clavelou P, Sandström G, Lund JP (2000) Evidence for functional compartmentalization of trigeminal muscle spindle afferents during fictive mastication in the rabbit. Eur J Neurosci 12:1145–1154.

Westneat MW, Hall WG (1992) Ontogeny of feeding motor patterns in infant rats: an electromyographic analysis of suckling and chewing. Behav Neurosci 106:539–554.

Wu N, Hsiao CF, Chandler SH (2001) Membrane resonance and subthreshold membrane oscillations in mesencephalic V neurons: participants in burst generation. J Neurosci 21:3729–3739.

Wu N, Enomoto A, Tanaka S, Hsiao CF, Nykamp DQ, Izhikevich E, Chandler SH (2005) Persistent sodium currents in mesencephalic V neurons participate in burst generation and control of membrane excitability. J Neurophysiol 93:2710–2722.

Zheng-Fischhöfer Q, Ghanem A, Kim JS, Kibschull M, Schwarz G, Schwab JO, Nagy J, Winterhager E, Tiemann K, Willecke K (2006) Connexin31 cannot functionally replace connexin43 during cardiac morphogenesis in mice. J Cell Sci 119:693–701.

Zheng-Fischhöfer Q, Kibschull M, Schnichels M, Kretz M, Petrasch-Parwez E, Strotmann J, Reucher H, Lynn BD, Nagy JI, Lye SJ, Winterhager E, Willecke K (2007a) Characterization of connexin31.1 deficient mice reveals impaired placental development. Dev Biol 312:258–271.

Zheng-Fischhöfer Q, Schnichels M, Dere E, Strotmann J, Loscher N, McCulloch F, Kretz M, Degen J, Reucher H, Nagy JI, Peti-Peterdi J, Huston JP, Breer H, Willecke K (2007b) Characterization of connexin30.3-deficient mice suggests a possible role of connexin30.3 in olfaction. Eur J Cell Biol 86:683–700.